arXiv:2511.01266v5 [cs.CV] 5 Mar 2026

MOTIONSTREAM: REAL-TIME VIDEO GENERATION WITH INTERACTIVE MOTION CONTROLS

Joonghyuk Shin[1,2] **Zhengqi Li**[2] **Richard Zhang**[2] **Jun-Yan Zhu**[3]
Jaesik Park[1] **Eli Shechtman**[2] **Xun Huang**[2,4]
[1]Seoul National University, [2]Adobe Research, [3]Carnegie Mellon University, [4]Morpheus AI

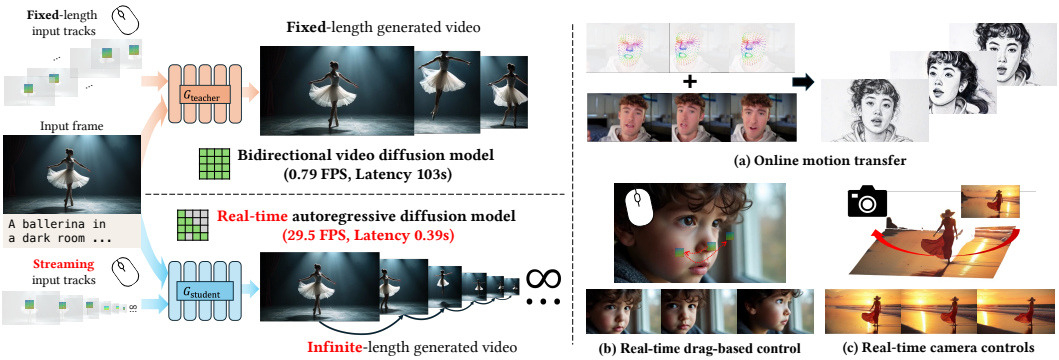


Figure 1: Prior motion-controlled video diffusion models typically operate offline to generate fixed-length sequences in parallel (top left). In contrast, our `MotionStream` enables streaming long-video generation from a single image with track control at interactive speed (bottom left). `MotionStream` can be applied to a variety of online downstream applications, such as real-time motion transfer, user drag operations, and 3D camera control (right).

ABSTRACT

Current motion-conditioned video generation methods suffer from prohibitive latency (minutes per video) and non-causal processing that prevents real-time interaction. We present `MotionStream`, enabling sub-second latency with up to 29 FPS streaming generation on a single GPU. Our approach begins by augmenting a text-to-video model with motion control, which generates high-quality videos that adhere to the global text prompt and local motion guidance, but does not perform inference on the fly. As such, we distill this bidirectional teacher into a causal student through Self Forcing with Distribution Matching Distillation, enabling real-time streaming inference. Several key challenges arise when generating videos of long, potentially infinite time-horizons – (1) bridging the domain gap from training on finite length and extrapolating to infinite horizons, (2) sustaining high quality by preventing error accumulation, and (3) maintaining fast inference, without incurring growth in computational cost due to increasing context windows. A key to our approach is introducing carefully designed sliding-window causal attention, combined with attention sinks. By incorporating self-rollout with attention sinks and KV cache rolling during training, we properly simulate inference-time extrapolations with a fixed context window, enabling constant-speed generation of arbitrarily long videos. Our models achieve state-of-the-art results in motion following and video quality while being two orders of magnitude faster, uniquely enabling infinite-length streaming. With `MotionStream`, users can paint trajectories, control cameras, or transfer motion, and see results unfold in real-time, delivering a truly interactive experience.

1 INTRODUCTION

The ultimate goal of motion-controlled video synthesis is to give creators the power of a director's chair, allowing them to intuitively guide digital actors, objects, and cameras in real time. Although recent video diffusion models have made impressive strides toward this goal (Wang et al., 2024b; Geng et al., 2025; Burgert et al., 2025; Zhang et al., 2025b; Li et al., 2025b;c; Niu et al., 2024; Shi et al., 2024a; Zhou et al., 2025a; Lei et al., 2025), generating high-fidelity videos following user-specified motion trajectories, the experience remains far from interactive.

The promise of interactive control is currently hindered by several fundamental constraints. First, generation is too slow for interaction. For example, synthesizing a 5-second video clip with Motion Prompting (Geng et al., 2025) takes 12 minutes, trapping users in frustrating "render-and-wait" cycles. Second, the process is inherently non-causal, since diffusion models process the entire sequence in parallel with bidirectional attention. A user cannot see any partial results until the entire motion specification is complete. Finally, the inability to generate more than a few seconds of video severely limits the scope for any meaningful or extended creative expression. Together, these constraints (slow, non-causal, and short-duration generation) undermine the potential for a truly interactive creative experience.

To overcome these challenges, we introduce `MotionStream`, a method designed specifically for an interactive creative experience. Unlike conventional diffusion models that operate on the entire video sequence in parallel, `MotionStream` is an autoregressive model that synthesizes video in a streaming manner, reacting to user-drawn motion trajectories on-the-fly.

Our approach starts with a motion-controlled teacher model that uses lightweight sinusoidal embeddings with channel-wise concatenation for trajectory conditioning, avoiding the computational overhead of ControlNet-style (Zhang et al., 2023) architectures. Trained on both text and motion conditions, we introduce joint text-motion guidance that balances precise trajectory adherence with natural secondary motions enabled by text prompts. We then distill this teacher into a causal student through Self Forcing-style self-rollout (Huang et al., 2025b). While effective for short sequences, standard approaches drift during extended generation. Our analysis of attention patterns reveals persistent focus on initial frames alongside local temporal dependencies, similar to StreamingLLM (Xiao et al., 2023). This insight drives our attention sinking mechanism with rolling KV caches, which we incorporate directly into training to properly simulate inference-time extrapolation distributions, ensuring stable, indefinite-length generation at constant latency through fixed context windows.

`MotionStream` achieves 17 FPS at 480P and 10 FPS at 720P resolutions with sub-second latency on a single H100 GPU, reaching 29 FPS when optimized with efficient VAE decoders that we specifically train for streaming applications. Through extensive experiments and ablations, we demonstrate state-of-the-art performance across diverse motion control tasks including camera control, where our approach outperforms recent 3D methods while being more than 20$\times$ faster. `MotionStream` transforms video generation from a passive waiting experience into an active creative process, where users can continuously interact with and guide the generation in real-time.

Our key contributions are:

1. We present the first *streaming* motion-conditioned video generation pipeline capable of running at 29.5 FPS on a single H100 GPU, enabling real-time interactive applications.

2. We propose a synergistic system harmonizing efficient architectural designs, including a lightweight track head and conditioning modules, with a distillation process that integrates joint text-motion guidance into the training objective, further accelerated by a Tiny VAE.

3. We introduce a distillation strategy for long video generation that systematically explores attention sinks and local attention with extrapolation-aware training for the first time, effectively preventing drift during long-term streaming.

4. Our approach achieves state-of-the-art results on motion transfer and camera control at orders of magnitude faster speeds, robustly generalizing to diverse interactive use cases.

2 RELATED WORK

Controllable Video Generation. Enabling precise user control is essential for applying video generative models to diverse downstream applications (Li et al., 2025d; Tu et al., 2025; Bahmani et al., 2024a; Gao et al., 2024c; Wu et al., 2025b; Fu et al., 2025). To this end, a large body of recent research has explored various types of control signals for video generation, such as structure control (Xing et al., 2024; Yang et al., 2025a; Jiang et al., 2025; Pang et al., 2024; Xing et al., 2025), camera control (Gao et al., 2024b; Zheng et al., 2024; He et al., 2024; Bai et al., 2025; Wu et al., 2025a; Yu et al., 2025b; Bahmani et al., 2024b; Yang et al., 2024b; Zheng et al., 2024; 2025), subject control (Huang et al., 2025a; Liu et al., 2025b; Fei et al., 2025; Liu et al., 2025a), and audio control (Tian et al., 2024; Gao et al., 2025; Peng et al., 2024).

As a unique modality that captures underlying video dynamics, motion has become a key conditioning signal for recent video diffusion models. Recent video diffusion models often condition generated videos on diverse forms of motion representations, including optical flow, 2D/3D motion trajectories, bounding boxes, and semantic segmentation (Goldman et al., 2008; Niu et al., 2024; Li et al., 2024; Wu et al., 2024b; Geng et al., 2025; Zhang et al., 2025b; Gillman et al., 2025; Shi et al., 2024a; Wu et al., 2024a; Gu et al., 2025b; Burgert et al., 2025; Tanveer et al., 2024). Despite their impressive quality, these methods are fundamentally limited to offline processing because they rely on diffusion models with full bidirectional attention, which requires the entire control signal to be known in advance. This constraint prevents their use in real-time, interactive applications.

Autoregressive Video Models. Early work adopted generative adversarial networks (GANs) for autoregressive or parallel video synthesis (Vondrick et al., 2016; Brooks et al., 2022; Villegas et al., 2017; Denton et al., 2017; Tulyakov et al., 2018; Liu et al., 2021; Li et al., 2022). More recently, there has been a paradigm shift towards using diffusion models trained with denoising objectives (Ho et al., 2022; Blattmann et al., 2023b; Yang et al., 2025b; Kong et al., 2024; Polyak et al., 2024; Blattmann et al., 2023a; Villegas et al., 2023; Deng et al., 2025; Gupta et al., 2024; Team Wan et al., 2025), or autoregressive (AR) models trained with next-token prediction (Weissenborn et al., 2020; Kondratyuk et al., 2024; Yan et al., 2021; Wang et al., 2024a; Bruce et al., 2024; Ren et al., 2025).

Another line of research integrates AR and diffusion to enable causal, high-quality video generation (Ruhe et al., 2024; Kim et al., 2024; Xie et al., 2024; Zhang & Agrawala, 2025; Sun et al., 2025; Weng et al., 2024; Liu et al., 2024; Chen et al., 2024; Guo et al., 2025b; Hu et al., 2024; Jin et al., 2025; Gu et al., 2025a; Gao et al., 2024a; Li et al., 2025f; Zhang et al., 2025a). Our work is inspired by the recent paradigm that distills a slow teacher model into a fast AR student for real-time performance (Yin et al., 2025; Huang et al., 2025b; Lin et al., 2025). However, these approaches either exhibit severe color drifts beyond the training horizon or require complex long-video finetuning, which poses challenges for controllable video generation.

Interactive Video World Model. Our work also belongs to interactive video world models, which aim to simulate environments for real-time interaction. This area has recently gained significant attention, as several recent works have shown impressive real-time, user-driven interaction (Ball et al., 2025; Li et al., 2025a; Yan Team, 2025; He et al., 2025; Bar et al., 2025; Po et al., 2025). However, most existing approaches either require substantial compute for inference (Ball et al., 2025; Parker-Holder et al., 2024), or are limited to closed-domain or synthetic environments (Yu et al., 2025a; Guo et al., 2025a; Yang et al., 2024a). In contrast, our work demonstrates that real-time, interactive generation for open-domain, photorealistic videos can be achieved on a single GPU.

3 MOTIONSTREAM: STREAMING GENERATION MEETS MOTION CONTROLS

Existing motion-conditioned video generation methods achieve strong motion-video alignment, but cannot support streaming interaction since bidirectional attention requires all future control signals upfront. Our proposed `MotionStream` addresses this through carefully designed causal distillation techniques, as illustrated in Figure 2. We first describe how to equip a pretrained video diffusion model with motion-control capability (Sec. 3.1) to serve as our bidirectional teacher, utilizing a lightweight track head and control modules designed to minimize architectural overhead. We then introduce our causal distillation pipeline, which performs extrapolation-aware training with attention sinks and local windows for long video generation, while integrating expensive joint text-

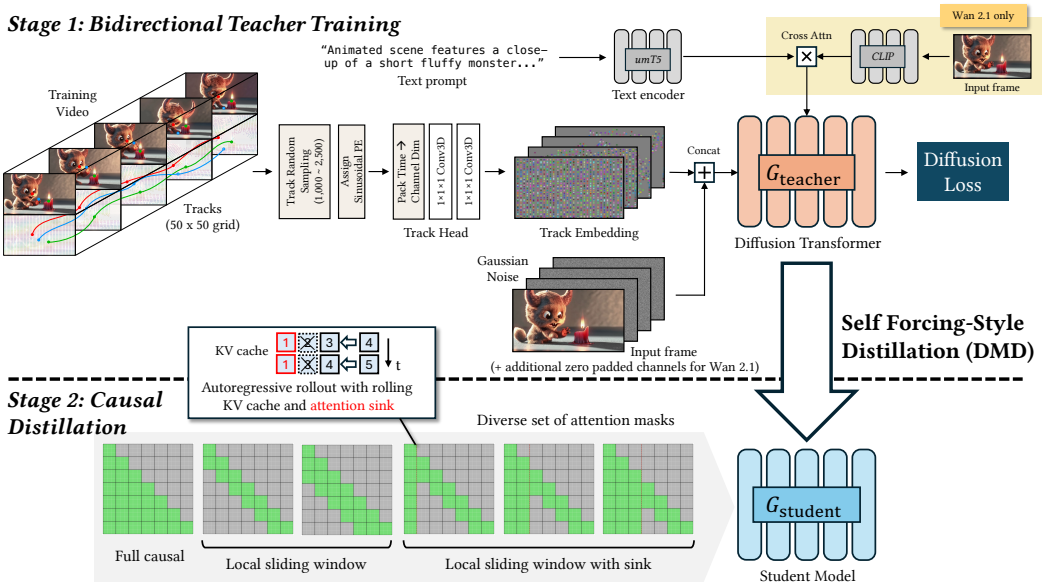


Figure 2: **Model architecture and training pipeline.** To build a teacher motion-controlled video model, we extract and randomly sample 2D tracks from the input video and encode them using a lightweight track head. The resulting track embeddings are combined with the input image, noisy video latents, and text embeddings as input to the diffusion transformer with bidirectional attention, which is then trained with a flow matching loss (top). We then distill a few-step causal diffusion model from the teacher through Self Forcing-style DMD distillation, integrating joint text-motion guidance into the objective, where autoregressive rollout with rolling KV cache and attention sink is applied during both training and inference (bottom).

motion guidance directly into the distillation objective for efficiency. Combined with our Tiny VAE, these joint efforts enable a highly responsive streaming experience.

3.1 Adding Motion Controls to Bidirectional Teacher Models

Training a high-quality motion-conditioned teacher model is important, as it determines both the quality upper bound and the architectural efficiency of the final distilled system. The teacher must also support diverse motion modalities, from complex real-world object dynamics to camera motions and user drags, which we achieve through the following design. We build our motion-guided teacher model on top of the Wan DiT family (Team Wan et al., 2025).

Track Representation and Track Head Design. Following MotionPrompting (Geng et al., 2025), each 2D track is assigned a unique d-dimensional embedding vector ϕ_n, derived from a randomly sampled ID number through sinusoidal positional encoding. While encoding tracks as an RGB video and processing it through the CausalVAE is possible, we find that representing them with sinusoidal embeddings with a learnable track head achieves superior track adherence, video quality, and faster speed. We validate this in our experiments in Table 3. Given N tracks $\{(x_t^n, y_t^n)\}_{n=1}^N$ across T temporal frames, the input track-conditioning signal $c_m \in \mathbb{R}^{T\times H/s\times W/s\times d}$ is constructed by placing visible track embeddings at spatially downsampled locations, where s is the VAE spatial downsampling rate and $v[t,n] \in \{0,1\}$ indicates track visibility:

$$c_m\left[t, \lfloor \tfrac{y_t^n}{s} \rfloor, \lfloor \tfrac{x_t^n}{s} \rfloor\right] = v[t,n] \cdot \phi_n. \tag{1}$$

Our lightweight track-encoding head performs $4\times$ temporal compression followed by a $1 \times 1 \times 1$ convolution. Prior methods adopt a ControlNet-style architecture (Zhang et al., 2023; Geng et al., 2025), which doubles FLOPs by duplicating network blocks. Instead, we directly concatenate the processed track embeddings with video latents, requiring only minor channel adjustments in the patchifying layer while leaving the core DiT architecture unchanged.

Training. We train the motion-guided teacher model through rectified flow matching objective (Liu et al., 2022; Lipman et al., 2022), where the forward process linearly interpolates between data z_0 and Gaussian noise $z_1 \sim \mathcal{N}(0, I)$: $z_t = (1-t)z_0 + tz_1,\ t \in [0, 1]$. The model is trained to predict the expected velocity fields with conditional flow matching loss $\mathcal{L}_{\text{FM}}$. One important limitation to note is that the model cannot inherently distinguish between occluded (non-visible) tracks and unspecified tracks, as both are represented by zero values. When a user releases controls during interaction, the model cannot determine whether the sudden zero values indicate occlusion or simply the absence of specification. This ambiguity occasionally leads to artifacts where objects abruptly appear or disappear. To address this issue, we introduce stochastic mid-frame masking with probability $p_{\text{mask}} = 0.2$, where $c_m[t_{\text{rand}}, :, :] = 0$, for randomly selected mid-frame chunks t_{rand}. In practice, we first train the model without masking to establish strong track-following capability, and then fine-tune with stochastic masking to preserve coherence when track signals change intermittently.

Joint Guidance with Text and Motion Conditions. Classifier-free guidance is an effective technique for steering diffusion models. We use both text and motion guidance and observe that they are complementary to each other. Text guidance generates natural dynamics but fails to maintain trajectory adherence. In contrast, track guidance enforces strict trajectory alignment but can produce overly simplistic and rigid motions, such as pure 2D planar translations in real-time drag scenarios. Therefore, we introduce a joint combination for simultaneous text and motion guidance:

$$\hat{v} = v_{\text{base}} + w_t \cdot \big(v(c_t, c_m) - v(\varnothing, c_m)\big) + w_m \cdot \big(v(c_t, c_m) - v(c_t, \varnothing)\big), \tag{2}$$

where $v_{\text{base}} = \alpha \cdot v(\varnothing, c_m) + (1-\alpha) \cdot v(c_t, \varnothing)$ and $\alpha = w_t/(w_t + w_m)$ (we omit z_t for brevity). We find that the joint guidance weights ($w_t = 3.0$, $w_m = 1.5$) provide a good balance: text conditioning enables realistic dynamics, even with sparse, flat-grid inputs, while track guidance preserves trajectories and maintains shape fidelity. We further analyze these effects in Sec. 4.3. Although this increases sampling cost from 2 to 3 function evaluations (NFE) per denoising step in the teacher model, our causal distillation (described in the next section) embeds all guidance into a single NFE, thereby eliminating this overhead in the student model.

3.2 Causal Distillation

Existing motion-controlled video diffusion models require around 50 denoising steps to generate high-quality video and also presume that the entire input motion trajectory is known before generation. In this section, we distill the slow teacher model into a causal video diffusion model, enabling real-time streaming of long videos with motion control. Our training pipeline starts from the Self Forcing paradigm (Huang et al., 2025b), but off-the-shelf, we find this exhibits large latency fluctuations due to varying attention window sizes and performs well only within the teacher's training horizon (*i.e.*, 81 frames), with quality quickly degrading when extrapolating to longer sequences. This section presents several key technical innovations to address these issues.

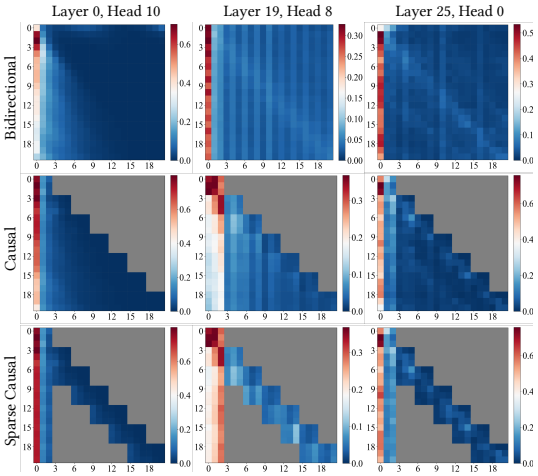


Figure 3: **Visualization of self attention probability map.** We visualize attention probability maps for bidirectional, full causal, and causal sliding window attentions. Several attention heads focus on the tokens corresponding to the initial frame throughout denoising generation.

Attention sink in video diffusion model. Autoregressive generation with sliding-window attention, as employed in Self Forcing (Huang et al., 2025b), is prone to quality degradation and drift during long-video extrapolation. To understand this failure, we visualize the self-attention maps in Figure 3 for both bidirectional and causal attention. Notably, many attention heads focus on the initial tokens corresponding to the input image. This phenomenon mirrors the observations in large language models Xiao et al. (2023), where initial tokens play a crucial role in stable streaming generation. Inspired by this, we adapt the attention sink concept to our video model by maintaining a local attention window while preserving the initial frame's tokens as a fixed anchor

during both training and inference. In our chunk-wise autoregressive setup, this sinking mechanism prevents the model from drifting during long-video extrapolation, even when trained only on short sequences limited by the teacher model.

Causal Adaptation. Following the initialization protocol from CausVid (Yin et al., 2025), we start our student model with the weights of the motion-guided teacher diffusion model and adapt it for causal attention architecture and few-step trajectory, using regression on ODE solution pairs sampled from the teacher. We train the model using attention masks with varying context window size and attention sink size for better generalization.

Self Forcing-Style Distillation. Following Self Forcing (Huang et al., 2025b), we perform temporal autoregressive roll-out with distribution matching distillation (DMD) (Yin et al., 2024b;a). During roll-out, video chunks are generated sequentially, conditioned on previously self-generated outputs rather than ground truth using KV cache.

We first define a video latent divided into L chunks as $\{z_t^i\}_{i=1}^L$, where t is the timestep. The sampling process of the i-th chunk can attend to its own noisy tokens and previously generated clean key and value tokens: $\mathcal{C}_i = \{z_t^i\} \cup \{z_0^j\}_{j \le S} \cup \{z_0^j\}_{\max(1,i-W) \le j < i}$, where S denotes the number of sink chunks, and W the attention window. Setting it to $\{z_t^i\} \cup \{z_0^j\}_{j<i}$ would correspond to a causal case with full history context window, matching that of Self Forcing. The generator G_θ produces each chunk autoregressively through the factorization $p_\theta(z_0^{1:L}) = \prod_{i=1}^L p_\theta(z_0^i|\mathcal{C}_i)$. Sampling each z_0^i involves K-step iterative denoising on its latent z_t^i, starting from pure noise $z_T^i \sim \mathcal{N}(0, I)$.

In our approach, because the KV cache is continuously updated, RoPE values are assigned based on cache position rather than absolute temporal index. We apply KV cache rolling with attention sinks during both training and inference, implementing local attention without explicit attention masking and fully bridging the train–test gap, even in *extrapolation* scenarios. While TalkingMachines (Low & Wang, 2025) also explores attention sinks, our method differs in two key aspects that enhance long-video stability. First, we eliminate the train-inference mismatch by explicitly simulating the extrapolation process during training, using self-rollout with a rolling KV cache and attention sinks. In contrast, TalkingMachines employs synchronized denoising with causal attention masks, which does not fully replicate the dynamics of autoregressive inference. Second, our training process ensures the teacher model always evaluates continuous video frames. The setup in TalkingMachines introduces a temporal discontinuity between the sink frame and subsequent frames, which can push the input outside the teacher's pre-training distribution. By maintaining continuity, our teacher provides more robust scores for distillation.

After generating all L chunks through self-rollout, we obtain the complete video $\hat{z}_0 = \{z_0^1, \ldots, z_0^L\}$. We then apply the DMD objective to this entire sequence, which minimizes the reverse KL divergence between the generator's output distribution and the data distribution: $\mathcal{L}_{\text{DMD}} = \mathbb{E}_t \left[D_{\text{KL}}(p_t^{\text{gen}} \| p_t^{\text{data}}) \right]$. The gradient with respect to the generator parameters θ becomes:

$$\nabla_\theta \mathcal{L}_{\text{DMD}} \approx -\mathbb{E}_{t,\hat{z}_0} \left[(s_{\text{real}}(\Psi(\hat{z}_0, t), t) - s_{\text{fake}}(\Psi(\hat{z}_0, t), t)) \cdot \frac{\partial \hat{z}_0}{\partial \theta} \right], \tag{3}$$

where s_{real} is the score function for real data (approximated by the frozen bidirectional teacher) and s_{fake} is the score function trained on the generator's outputs.

Intuitively, the driving gradient for the few-step causal generator G_θ comes from the difference between the estimated real and fake scores. To transfer the high-fidelity control of our joint guidance into the student without inference overhead, we define the target real score s_{real} using the frozen teacher f_ϕ with joint guidance (omitting z_t for brevity):

$$s_{\text{real}} = s_{\text{base}} + w_t \cdot (f_\phi(c_t, c_m) - f_\phi(\emptyset, c_m)) + w_m \cdot (f_\phi(c_t, c_m) - f_\phi(c_t, \emptyset)), \tag{4}$$

where s_{base} follows the weighting defined in Eq. 2. In contrast, we parameterize the fake score s_{fake} without using any CFG through a trainable critic f_ψ (which approximates the generator's score): $s_{\text{fake}} = f_\psi(c_t, c_m)$. This configuration effectively "bakes" the computational cost of the teacher's multi-term guidance into the distillation objective, allowing the student generator to replicate the high-quality joint-guided distribution with a single function evaluation.

We update the generator (G_θ) and fake score estimator (f_ψ) with a ratio of 1:5 (Yin et al., 2024a), allowing the critic to better approximate generated distributions. To reduce the memory usage during

Table 1: **Benchmark on Motion Transfer (Reconstruction).**

Method	Backbone & Resolution	FPS	DAVIS Validation Set				Sora Demo Subset			
			PSNR	SSIM	LPIPS	EPE	PSNR	SSIM	LPIPS	EPE
Image Conductor (Li et al., 2025e)	AnimateDiff (256P)	2.98	11.30	0.214	0.664	91.64	10.29	0.192	0.644	31.22
Go-With-The-Flow (Burgert et al., 2025)	CogVideoX-5B (480P)	0.60	15.62	0.392	0.490	41.99	14.59	0.410	0.425	10.27
Diffusion-As-Shader (Gu et al., 2025b)	CogVideoX-5B (480P)	0.29	15.80	0.372	0.483	40.23	14.51	0.382	0.437	18.76
ATI (Wang et al., 2025a)	Wan 2.1-14B (480P)	0.23	15.33	0.374	0.473	17.41	16.04	0.502	0.366	6.12
Ours Teacher (Joint CFG)	Wan 2.1-1.3B (480P)	0.79	**16.61**	**0.477**	**0.427**	**5.35**	**17.82**	**0.586**	0.333	**2.71**
Ours Causal (Distilled)	Wan 2.1-1.3B (480P)	**16.7**	16.20	0.447	0.443	7.80	16.67	0.531	0.360	4.21
Ours Teacher (Joint CFG)	Wan 2.2-5B (720P)	0.74	16.10	0.466	**0.427**	7.86	17.18	0.571	**0.331**	3.16
Ours Causal (Distilled)	Wan 2.2-5B (720P)	10.4	16.30	0.456	0.438	11.18	16.62	0.545	0.343	4.30

self-rollout, we adopt Self Forcing's gradient truncation strategy: randomly sampling denoising step k from $[1, K]$ and using the denoised output at k-th step as the final output, enabling gradient backpropagation only through that step. By additionally treating the cached KV from previous frames as stop-gradient context (detached), we track gradients only for the selected denoising step of the current block, effectively reducing the memory usage.

Inference. Our inference procedure identically follows the training process to ensure a perfect train-test match. We maintain a KV cache composed of S chunks from the initial frames and a fixed-size local window of recent W chunks. As new tokens are generated, this local window is "rolled" to maintain a constant size. For positional encoding, we store the final, RoPE-applied values for the static sink tokens, while tokens in the rolling window store pre-RoPE activations and receive positional indices dynamically based on their current cache location. Because this entire mechanism is simulated during training, the model seamlessly handles the discontinuity between sink and window tokens. This approach yields two key advantages over full-context methods: (1) initial image anchoring prevents drift during long rollouts, and (2) throughput and latency remain constant regardless of generated video length. We analyze the effects of attention sink and window size in Sec. 4.3 and describe our streaming pipeline in Sec. 4.4.

4 Experiments

4.1 Implementation Details

We build upon image-to-video (I2V) variants of Wan 2.1 (1.3B) and Wan 2.2 (5B) (Team Wan et al., 2025). We train teacher models on OpenVid-1M (Nan et al., 2024) and synthetic data generated by Wan text-to-video (T2V) model: Wan 2.1 at 832×480 (70K synthetic samples) and Wan 2.2 at 1280×704 (30K synthetic samples). For causal adaptation and Self Forcing distillation, we sample input images, text prompts and 2D tracks from the synthetic datasets described above. For computational efficiency, we track all real and synthetic videos from a 50×50 uniform grid with CoTracker3 (Karaev et al., 2024). We refer readers to Appendix for additional details.

4.2 Quantitative Evaluations

Motion Transfer. We evaluate motion-following capability on two datasets: the DAVIS (Perazzi et al., 2016) validation set (30 videos) and 20 curated videos from the Sora webpage (Brooks et al., 2024). We use both because DAVIS presents challenging sequences with significant occlusions, while the Sora set provides clean examples with consistent visibility, ensuring a comprehensive evaluation. We directly compare the synthesized results with the corresponding ground-truth video frames. Visual fidelity is measured using PSNR, SSIM, and LPIPS (Zhang et al., 2018), while motion accuracy is assessed via End-Point Error (EPE), computed as the L2 distance between visible input tracks and the tracks extracted from the generated videos. All models are evaluated in their optimal configuration, and evaluations are performed at 832×480 resolution after resizing. Speed measures are based on a single H100 GPU. We refer readers to Appendix for detailed protocols.

Camera Control. To assess our model's ability to generate videos following camera controls, we evaluate its zero-shot performance on single-image 3D novel view synthesis. We compare it against several recent diffusion- and feed-forward-based view synthesis baselines (Zhou et al., 2025b; Yu et al., 2024; Xu et al., 2025) on the LLFF dataset (Mildenhall et al., 2019). To adapt our 2D track-controlled model for this task, we first es-

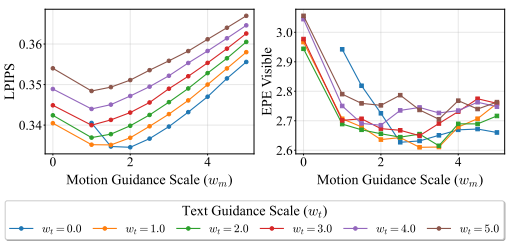


Figure 4: **Quantitative ablation on guidance.** We use Sora subset to ablate guidance strategies. Higher text guidance reduces overall metrics while motion guidance improves trajectory accuracy at the cost of visual quality (LPIPS).

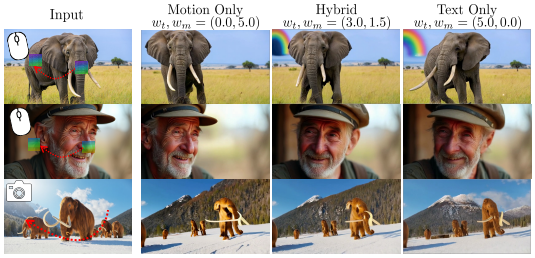


Figure 5: **Qualitative ablation on guidance.** Pure motion guidance produces rigid movements while text guidance enables natural motion and shape preservation even with imperfect tracks. Our *Hybrid* joint guidance balances these two.

timate scene geometry using a monocular depth network (Wang et al., 2025b) and compute a single scale factor to align the predicted depth with the reconstructed scene point cloud from COLMAP (Schonberger & Frahm, 2016). We then derive 2D motion trajectories by interpolating between the input and target frame using depth and camera parameters. For all methods, the input image aspect ratio is fixed at 16:9, and all synthesized frames are resized to 512×288 before evaluation with PSNR, SSIM, and LPIPS metrics. As shown in Table 2, our track-conditioned video generation models outperform other 3D novel view synthesis baselines by a large margin, even though they are not specifically designed for this task. Moreover, our causal models achieve significantly higher generation throughput compared with both the baselines and their bidirectional counterparts.

Table 2: **Evaluation on Novel View Synthesis.**

Method	Resolution	FPS	LLFF		
			PSNR	SSIM	LPIPS
DepthSplat (Xu et al., 2025)	576P	1.40	13.9	0.28	0.30
ViewCrafter (Yu et al., 2024)	576P	0.26	14.0	0.30	0.30
SEVA (Zhou et al., 2025b)	576P	0.20	14.1	0.30	0.29
Ours Teacher (1.3B)	480P	0.79	**16.0**	**0.42**	**0.21**
Ours Causal (1.3B)	480P	**16.7**	<u>15.7</u>	0.38	0.23
Ours Teacher (5B)	720P	0.74	14.0	<u>0.40</u>	<u>0.22</u>
Ours Causal (5B)	720P	<u>10.4</u>	15.0	0.39	0.23

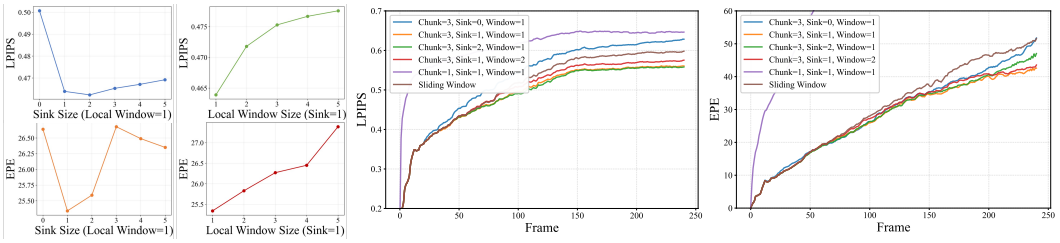
4.3 Ablation Experiments

Track Representation. We compare our sinusoidal position encoding with a learnable track head against the RGB encoding strategy using a frozen VAE, following prior work (Gu et al., 2025b), where each 2D track is assigned a unique RGB color vector and placed onto a canvas before being fed into the VAE. Table 3 shows that our method (PE-Head) outperforms RGB-VAE in both efficiency and quality. Specifically, our lightweight PE-based encoding achieves better motion alignment while being two orders of magnitude faster than the VAE-based approach. We hypothesize sinusoidal encoding preserves stronger identification signals compared to RGB encoding due to richer expressive dimensions.

Table 3: **Comparing track representation methods.** Our sinusoidal PE with learnable track head outperforms RGB-VAE in both quality and efficiency, achieving 40× faster encoding critical for real-time streaming.

Method	Time (ms)	DAVIS / Sora			
		PSNR	SSIM	LPIPS	EPE
RGB-VAE	1053	16.03 / 16.99	0.433 / 0.544	0.463 / 0.363	8.57 / 3.96
PE-Head	**24.8**	**16.29 / 17.15**	**0.452 / 0.559**	**0.456 / 0.359**	**6.54 / 3.13**

Guidance Strategies. Here we ablate our joint guidance approach from Sec.3.1. While pure motion guidance ($w_t = 0$, $w_m > 0$) achieves the highest trajectory accuracy, as shown in Figure 4, text guidance provides additional benefits for generating more diverse and realistic results. For example, text captions enable dynamics beyond trajectories alone, such as weather changes or object appearances as shown in the first row of Figure 5, which illustrates dragging an elephant while prompting "rainbow appears in background". Our empirical setting ($w_t = 3.0$, $w_m = 1.5$) balances motion fidelity with natural dynamics, adapting equally well to both precise and imperfect trajectories.



(a) Impact of Sink Size & Local Window Size (b) LPIPS Over Time Across Diverse Setups (c) EPE Over Time Across Diverse Setups

Figure 6: **Impact of Sparse Attention Patterns.** Using longer clips (up to 241 frames) from the Sora subset, we ablate attention sink size and local window size in extrapolation scenarios. Having at least a single sink chunk is crucial, but more provides marginal benefit, while larger window sizes degrade performance as attending to long-past history allows errors to accumulate in context tokens.

Impact of Chunk Size, Attention Sink, and Window Size. We investigate three key design choices that govern streaming quality and interactivity: the latent chunk size, the attention sink size, and the local context window size.

The chunk size, which defines how many video latents are processed in parallel, presents a critical trade-off between quality, latency, and throughput. As illustrated in the latency-throughput analysis in Figure A2, small chunks lead to lower throughput, while large chunks (>3) introduce prohibitive latency for real-time interaction. Additionally, as shown in Tab. 4, a chunk size of 1 causes significant quality degradation. We, therefore, select a chunk size of 3 as our optimal configuration, with further analysis provided in Appendix Sec. C.

To assess the impact of attention sinks and window size on model performance, we train a single model with randomly sampled sink and window sizes and then generate videos under different configuration combinations. We evaluate long-video extrapolation on Sora videos up to 241 frames (average 194 frames). Surprisingly, we find that the minimal configuration (a single-chunk sink with a single-chunk window) achieves the best performance. Figure 6(a) shows that additional sinks provide only marginal gains while increasing latency, and expanded windows actually degrade performance. We hypothesize that this phenomenon arises because restricting the context to immediate predecessors, rather than long-past history, prevents error accumulation and thus reduces drift for long-video generation.

Table 4: **Ablation study on Sora Extended.** `c3s1w1` maintains high visual quality with small latency & throughput fluctuations, while vanilla sliding window exhibits large fluctuations degrading streaming stability.

Config	Sora Extended			
	LPIPS	EPE	Latency (s)	Throughput (FPS)
Ours base (`c3s1w1`)	**0.464**	**25.34**	0.70 ± 0.01	16.92 ± 0.80
+ Remove sink (`c3s0w1`)	0.501	26.64	0.68 ± 0.005	**17.43 ± 0.88**
+ Chunk Size 1 (`c1s1w1`)	0.597	76.21	**0.30 ± 0.01**	13.26 ± 1.36
Sliding window	0.480	28.09	0.80 ± 0.08	14.96 ± 1.42

We additionally show reconstruction accuracy and throughput as well as their time evolution in Table 4 and Figure 6(b,c) respectively. We denote our configuration as `chunk-3, sink-1, window-1` (abbreviated `c3s1w1`), while sliding window approach used in Self Forcing is `c3s0w6`, attending to a maximum of 6 previous chunks without sink tokens, with unbounded RoPE positions that scale with temporal frame count. Although removing sink tokens (`c3s0w1`) yields marginal speed improvements, this comes at the cost of degraded long-term generation stability.

4.4 Streaming Demo and Qualitative Results

For streaming demos, we further optimize the pipeline with an efficient Tiny VAE. Inspired by Boer Bohan (2025), we design and train a smaller VAE decoder with adversarial and LPIPS losses, regressing to the original VAE's latent space. Tiny VAE removes the VAE bottleneck by reducing the decoding time over 10×, improving Wan 2.1 from 16.7 FPS with 0.69s latency to 29.5 FPS with 0.39s latency, and Wan 2.2 from 10.4 FPS with 1.1s latency to 23.9 FPS with 0.49s latency on a single H100 GPU. We provide details for the tiny VAE in Appendix A, noting that the performance trade-off from switching to the tiny VAE is marginal in streaming scenarios, as shown

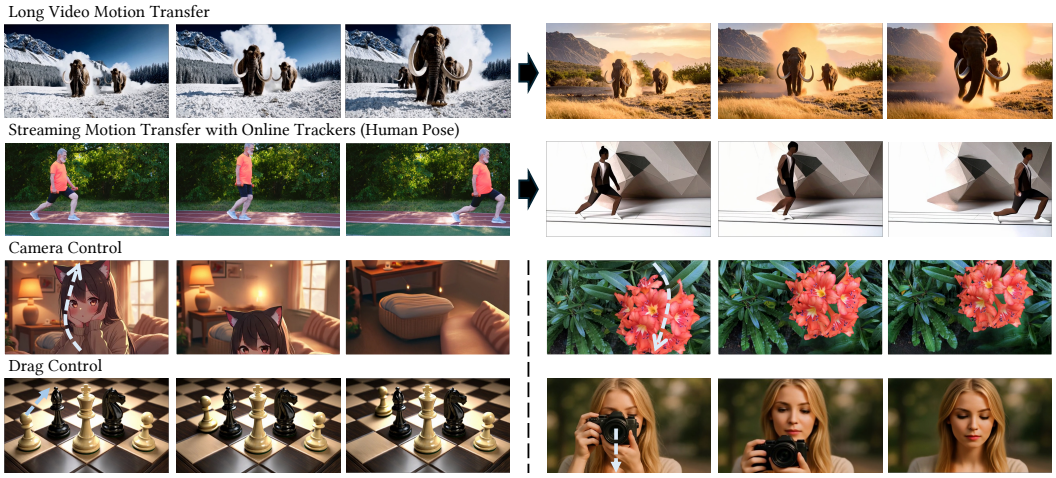


Figure 7: **Qualitative Results.** `MotionStream` can perform diverse downstream applications, including long video motion transfer (from offline or online sources), drag-based controls, and precise camera control with depth estimation. We showcase a few examples here.

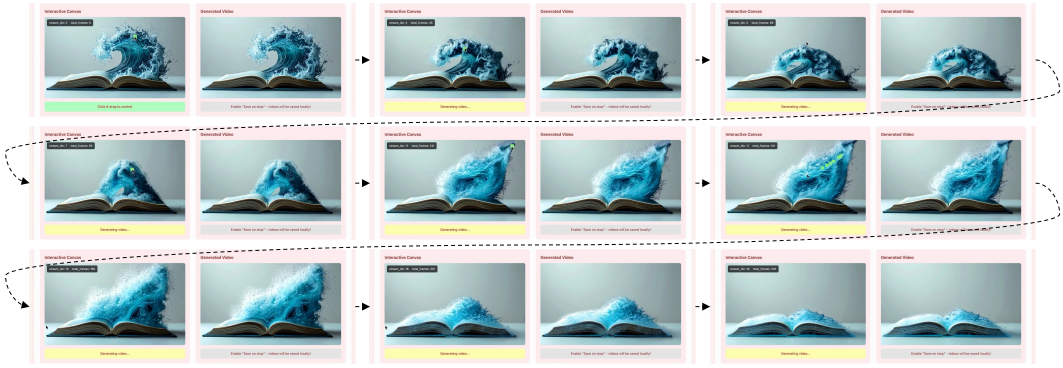


Figure 8: **Streaming Demo.** An example of real-time streaming generation; more details in Sec. C.

in Table A2. Leveraging track representation, our method enables causal, real-time execution of capabilities typically found in motion control approaches, such as mouse-based drag control and motion transfer using tracks from online trackers. Figure 7 demonstrates several of these applications. Additionally, we develop an interactive demo that enables real-time user control during streaming generation. Figure 8 shows an example, with further details in Sec. C and Figure A5.

5 Conclusion

We propose `MotionStream`, a framework for infinite-length video generation with interactive motion control, maintaining a stable 29 FPS on a single GPU. Our contributions span from training a motion-guided teacher with efficient track head and joint text-motion guidance, to distilling it into a causal student via self-rollout with attention sink and rolling KV caches. `MotionStream` achieves state-of-the-art results across diverse motion-conditioned generation tasks, while being significantly faster than prior methods. Limitations and future directions, as well as ethics and reproducibility statements are discussed in Appendix F and G.

Acknowledgments. This work was done at Adobe Research, during Joonghyuk Shin's internship and while Xun Huang was a Research Scientist. Jaesik Park was supported by the IITP grant No. RS-2021-II211343 (Artificial Intelligence Graduate School Program at Seoul National University, 5%), No. RS-2025-25442338 (AI Star Fellowship Support Program, 35%), and the NRF grant No. RS-2024-00405857 (60%) funded by the Korea government (MSIT). Jun-Yan Zhu was supported by the Packard Fellowship.

REFERENCES

AIGC-Apps and Alibaba PAI Team. VideoX-Fun: A Flexible Framework for Video Generation at Any Resolution. https://github.com/aigc-apps/VideoX-Fun, 2024.

Sherwin Bahmani, Ivan Skorokhodov, Victor Rong, Gordon Wetzstein, Leonidas Guibas, Peter Wonka, Sergey Tulyakov, Jeong Joon Park, Andrea Tagliasacchi, and David B Lindell. 4d-fy: Text-to-4d generation using hybrid score distillation sampling. In *Proceedings of the IEEE/CVF Conference on Computer Vision and Pattern Recognition*, pp. 7996–8006, 2024a.

Sherwin Bahmani, Ivan Skorokhodov, Aliaksandr Siarohin, Willi Menapace, Guocheng Qian, Michael Vasilkovsky, Hsin-Ying Lee, Chaoyang Wang, Jiaxu Zou, Andrea Tagliasacchi, et al. Vd3d: Taming large video diffusion transformers for 3d camera control. *arXiv preprint arXiv:2407.12781*, 2024b.

Jianhong Bai, Menghan Xia, Xiao Fu, Xintao Wang, Lianrui Mu, Jinwen Cao, Zuozhu Liu, Haoji Hu, Xiang Bai, Pengfei Wan, et al. Recammaster: Camera-controlled generative rendering from a single video. *arXiv preprint arXiv:2503.11647*, 2025.

Philip J Ball, J Bauer, F Belletti, et al. Genie 3: A new frontier for world models, 2025.

Amir Bar, Gaoyue Zhou, Danny Tran, Trevor Darrell, and Yann LeCun. Navigation world models. In *Proceedings of the Computer Vision and Pattern Recognition Conference*, pp. 15791–15801, 2025.

Andreas Blattmann, Tim Dockhorn, Sumith Kulal, Daniel Mendelevitch, Maciej Kilian, Dominik Lorenz, Yam Levi, Zion English, Vikram Voleti, Adam Letts, et al. Stable video diffusion: Scaling latent video diffusion models to large datasets. *arXiv preprint arXiv:2311.15127*, 2023a.

Andreas Blattmann, Robin Rombach, Huan Ling, Tim Dockhorn, Seung Wook Kim, Sanja Fidler, and Karsten Kreis. Align your latents: High-resolution video synthesis with latent diffusion models. In *CVPR*, 2023b.

Ollin Boer Bohan. Taehv: Tiny autoencoder for hunyuan video. `https://github.com/madebyollin/taehv`, 2025.

Tim Brooks, Janne Hellsten, Miika Aittala, Ting-Chun Wang, Timo Aila, Jaakko Lehtinen, Ming-Yu Liu, Alexei Efros, and Tero Karras. Generating long videos of dynamic scenes. *NeurIPS*, 2022.

Tim Brooks, Bill Peebles, Connor Holmes, Will DePue, Yufei Guo, Li Jing, David Schnurr, Joe Taylor, Troy Luhman, Eric Luhman, Clarence Ng, Ricky Wang, and Aditya Ramesh. Video generation models as world simulators, 2024. URL `https://openai.com/research/video-generation-models-as-world-simulators`.

Jake Bruce, Michael D Dennis, Ashley Edwards, Jack Parker-Holder, Yuge Shi, Edward Hughes, Matthew Lai, Aditi Mavalankar, Richie Steigerwald, Chris Apps, et al. Genie: Generative interactive environments. In *ICML*, 2024.

Ryan Burgert, Yuancheng Xu, Wenqi Xian, Oliver Pilarski, Pascal Clausen, Mingming He, Li Ma, Yitong Deng, Lingxiao Li, Mohsen Mousavi, et al. Go-with-the-flow: Motion-controllable video diffusion models using real-time warped noise. In *CVPR*, 2025.

Boyuan Chen, Diego Martí Monsó, Yilun Du, Max Simchowitz, Russ Tedrake, and Vincent Sitzmann. Diffusion forcing: Next-token prediction meets full-sequence diffusion. In *NeurIPS*, 2024.

June Suk Choi, Kyungmin Lee, Sihyun Yu, Yisol Choi, Jinwoo Shin, and Kimin Lee. Enhancing motion dynamics of image-to-video models via adaptive low-pass guidance. *arXiv preprint arXiv:2506.08456*, 2025.

Haoge Deng, Ting Pan, Haiwen Diao, Zhengxiong Luo, Yufeng Cui, Huchuan Lu, Shiguang Shan, Yonggang Qi, and Xinlong Wang. Autoregressive video generation without vector quantization. In *ICLR*, 2025.

Emily L Denton et al. Unsupervised learning of disentangled representations from video. In *NeurIPS*, 2017.

Zhengcong Fei, Debang Li, Di Qiu, Jiahua Wang, Yikun Dou, Rui Wang, Jingtao Xu, Mingyuan Fan, Guibin Chen, Yang Li, et al. Skyreels-a2: Compose anything in video diffusion transformers. *arXiv preprint arXiv:2504.02436*, 2025.

Xiao Fu, Xintao Wang, Xian Liu, Jianhong Bai, Runsen Xu, Pengfei Wan, Di Zhang, and Dahua Lin. Learning video generation for robotic manipulation with collaborative trajectory control. *arXiv preprint arXiv:2506.01943*, 2025.

Kaifeng Gao, Jiaxin Shi, Hanwang Zhang, Chunping Wang, Jun Xiao, and Long Chen. Ca2-vdm: Efficient autoregressive video diffusion model with causal generation and cache sharing. *arXiv preprint arXiv:2411.16375*, 2024a.

Ruiqi Gao, Aleksander Holynski, Philipp Henzler, Arthur Brussee, Ricardo Martin-Brualla, Pratul Srinivasan, Jonathan T Barron, and Ben Poole. Cat3d: Create anything in 3d with multi-view diffusion models. *arXiv preprint arXiv:2405.10314*, 2024b.

Shenyuan Gao, Jiazhi Yang, Li Chen, Kashyap Chitta, Yihang Qiu, Andreas Geiger, Jun Zhang, and Hongyang Li. Vista: A generalizable driving world model with high fidelity and versatile controllability. *Advances in Neural Information Processing Systems*, 37:91560–91596, 2024c.

Xin Gao, Li Hu, Siqi Hu, Mingyang Huang, Chaonan Ji, Dechao Meng, Jinwei Qi, Penchong Qiao, Zhen Shen, Yafei Song, Ke Sun, Linrui Tian, Guangyuan Wang, Qi Wang, Zhongjian Wang, Jiayu Xiao, Sheng Xu, Bang Zhang, Peng Zhang, Xindi Zhang, Zhe Zhang, Jingren Zhou, and Lian Zhuo. Wan-s2v: Audio-driven cinematic video generation, 2025. URL https://arxiv.org/abs/2508.18621.

Daniel Geng, Charles Herrmann, Junhwa Hur, Forrester Cole, Serena Zhang, Tobias Pfaff, Tatiana Lopez-Guevara, Yusuf Aytar, Michael Rubinstein, Chen Sun, et al. Motion prompting: Controlling video generation with motion trajectories. In *CVPR*, 2025.

Nate Gillman, Charles Herrmann, Michael Freeman, Daksh Aggarwal, Evan Luo, Deqing Sun, and Chen Sun. Force prompting: Video generation models can learn and generalize physics-based control signals. *arXiv preprint arXiv:2505.19386*, 2025.

Dan B Goldman, Chris Gonterman, Brian Curless, David Salesin, and Steven M Seitz. Video object annotation, navigation, and composition. In *Proceedings of the 21st annual ACM symposium on User interface software and technology*, pp. 3–12, 2008.

Yuchao Gu, Weijia Mao, and Mike Zheng Shou. Long-context autoregressive video modeling with next-frame prediction. *arXiv preprint arXiv:2503.19325*, 2025a.

Zekai Gu, Rui Yan, Jiahao Lu, Peng Li, Zhiyang Dou, Chenyang Si, Zhen Dong, Qifeng Liu, Cheng Lin, Ziwei Liu, et al. Diffusion as shader: 3d-aware video diffusion for versatile video generation control. In *Proceedings of the Special Interest Group on Computer Graphics and Interactive Techniques Conference Conference Papers*, pp. 1–12, 2025b.

Junliang Guo, Yang Ye, Tianyu He, Haoyu Wu, Yushu Jiang, Tim Pearce, and Jiang Bian. Mineworld: a real-time and open-source interactive world model on minecraft. *arXiv preprint arXiv:2504.08388*, 2025a.

Yuwei Guo, Ceyuan Yang, Ziyan Yang, Zhibei Ma, Zhijie Lin, Zhenheng Yang, Dahua Lin, and Lu Jiang. Long context tuning for video generation. *arXiv preprint arXiv:2503.10589*, 2025b.

Agrim Gupta, Lijun Yu, Kihyuk Sohn, Xiuye Gu, Meera Hahn, Fei-Fei Li, Irfan Essa, Lu Jiang, and José Lezama. Photorealistic video generation with diffusion models. In *ECCV*, 2024.

Hao He, Yinghao Xu, Yuwei Guo, Gordon Wetzstein, Bo Dai, Hongsheng Li, and Ceyuan Yang. Cameractrl: Enabling camera control for text-to-video generation. *arXiv preprint arXiv:2404.02101*, 2024.

Xianglong He, Chunli Peng, Zexiang Liu, Boyang Wang, Yifan Zhang, Qi Cui, Fei Kang, Biao Jiang, Mengyin An, Yangyang Ren, et al. Matrix-game 2.0: An open-source, real-time, and streaming interactive world model. *arXiv preprint arXiv:2508.13009*, 2025.

Jonathan Ho, Tim Salimans, Alexey Gritsenko, William Chan, Mohammad Norouzi, and David J Fleet. Video diffusion models. In *NeurIPS*, 2022.

Jinyi Hu, Shengding Hu, Yuxuan Song, Yufei Huang, Mingxuan Wang, Hao Zhou, Zhiyuan Liu, Wei-Ying Ma, and Maosong Sun. Acdit: Interpolating autoregressive conditional modeling and diffusion transformer. *arXiv preprint arXiv:2412.07720*, 2024.

Chi-Pin Huang, Yen-Siang Wu, Hung-Kai Chung, Kai-Po Chang, Fu-En Yang, and Yu-Chiang Frank Wang. Videomage: Multi-subject and motion customization of text-to-video diffusion models. In *Proceedings of the Computer Vision and Pattern Recognition Conference*, pp. 17603–17612, 2025a.

Xun Huang, Zhengqi Li, Guande He, Mingyuan Zhou, and Eli Shechtman. Self forcing: Bridging the train-test gap in autoregressive video diffusion. *arXiv preprint arXiv:2506.08009*, 2025b.

Ziqi Huang, Yinan He, Jiashuo Yu, Fan Zhang, Chenyang Si, Yuming Jiang, Yuanhan Zhang, Tianxing Wu, Qingyang Jin, Nattapol Chanpaisit, et al. Vbench: Comprehensive benchmark suite for video generative models. In *Proceedings of the IEEE/CVF Conference on Computer Vision and Pattern Recognition*, pp. 21807–21818, 2024.

Lifan Jiang, Shuang Chen, Boxi Wu, Xiaotong Guan, and Jiahui Zhang. Vidsketch: Hand-drawn sketch-driven video generation with diffusion control. *arXiv preprint arXiv:2502.01101*, 2025.

Yang Jin, Zhicheng Sun, Ningyuan Li, Kun Xu, Hao Jiang, Nan Zhuang, Quzhe Huang, Yang Song, Yadong Mu, and Zhouchen Lin. Pyramidal flow matching for efficient video generative modeling. In *ICLR*, 2025.

Nikita Karaev, Iurii Makarov, Jianyuan Wang, Natalia Neverova, Andrea Vedaldi, and Christian Rupprecht. Cotracker3: Simpler and better point tracking by pseudo-labelling real videos. *arXiv preprint arXiv:2410.11831*, 2024.

Jihwan Kim, Junoh Kang, Jinyoung Choi, and Bohyung Han. Fifo-diffusion: Generating infinite videos from text without training. *Advances in Neural Information Processing Systems*, 37: 89834–89868, 2024.

Diederik P Kingma and Jimmy Ba. Adam: A method for stochastic optimization. In *ICLR*, 2015.

Dan Kondratyuk, Lijun Yu, Xiuye Gu, Jose Lezama, Jonathan Huang, Grant Schindler, Rachel Hornung, Vighnesh Birodkar, Jimmy Yan, Ming-Chang Chiu, et al. Videopoet: A large language model for zero-shot video generation. In *ICML*, 2024.

Weijie Kong, Qi Tian, Zijian Zhang, Rox Min, Zuozhuo Dai, Jin Zhou, Jiangfeng Xiong, Xin Li, Bo Wu, Jianwei Zhang, et al. Hunyuanvideo: A systematic framework for large video generative models. *arXiv preprint arXiv:2412.03603*, 2024.

Guojun Lei, Chi Wang, Rong Zhang, Yikai Wang, Hong Li, and Weiwei Xu. Animateanything: Consistent and controllable animation for video generation. In *CVPR*, 2025.

Jiaqi Li, Junshu Tang, Zhiyong Xu, Longhuang Wu, Yuan Zhou, Shuai Shao, Tianbao Yu, Zhiguo Cao, and Qinglin Lu. Hunyuan-gamecraft: High-dynamic interactive game video generation with hybrid history condition. *arXiv preprint arXiv:2506.17201*, 2025a.

Quanhao Li, Zhen Xing, Rui Wang, Hui Zhang, Qi Dai, and Zuxuan Wu. Magicmotion: Controllable video generation with dense-to-sparse trajectory guidance. In *ICCV*, 2025b.

Ruining Li, Chuanxia Zheng, Christian Rupprecht, and Andrea Vedaldi. Puppet-master: Scaling interactive video generation as a motion prior for part-level dynamics. In *Proceedings of the IEEE/CVF International Conference on Computer Vision*, pp. 13405–13415, 2025c.

Xiaowen Li, Haolan Xue, Peiran Ren, and Liefeng Bo. Diffueraser: A diffusion model for video inpainting. *arXiv preprint arXiv:2501.10018*, 2025d.

Yaowei Li, Xintao Wang, Zhaoyang Zhang, Zhouxia Wang, Ziyang Yuan, Liangbin Xie, Ying Shan, and Yuexian Zou. Image conductor: Precision control for interactive video synthesis. In *AAAI*, 2025e.

Zhengqi Li, Qianqian Wang, Noah Snavely, and Angjoo Kanazawa. Infinitenature-zero: Learning perpetual view generation of natural scenes from single images. In *ECCV*, 2022.

Zhengqi Li, Richard Tucker, Noah Snavely, and Aleksander Holynski. Generative image dynamics. In *Proceedings of the IEEE/CVF Conference on Computer Vision and Pattern Recognition*, pp. 24142–24153, 2024.

Zongyi Li, Shujie Hu, Shujie Liu, Long Zhou, Jeongsoo Choi, Lingwei Meng, Xun Guo, Jinyu Li, Hefei Ling, and Furu Wei. Arlon: Boosting diffusion transformers with autoregressive models for long video generation. In *ICLR*, 2025f.

Shanchuan Lin, Xin Xia, Yuxi Ren, Ceyuan Yang, Xuefeng Xiao, and Lu Jiang. Diffusion adversarial post-training for one-step video generation. *arXiv preprint arXiv:2501.08316*, 2025.

Yaron Lipman, Ricky TQ Chen, Heli Ben-Hamu, Maximilian Nickel, and Matt Le. Flow matching for generative modeling. *arXiv preprint arXiv:2210.02747*, 2022.

Andrew Liu, Richard Tucker, Varun Jampani, Ameesh Makadia, Noah Snavely, and Angjoo Kanazawa. Infinite nature: Perpetual view generation of natural scenes from a single image. In *ICCV*, 2021.

Lijie Liu, Tianxiang Ma, Bingchuan Li, Zhuowei Chen, Jiawei Liu, Gen Li, Siyu Zhou, Qian He, and Xinglong Wu. Phantom: Subject-consistent video generation via cross-modal alignment. *arXiv preprint arXiv:2502.11079*, 2025a.

Xiaoyu Liu, Mingshuai Yao, Yabo Zhang, Xianhui Lin, Peiran Ren, Xiaoming Li, Ming Liu, and Wangmeng Zuo. Animateanywhere: Rouse the background in human image animation. *arXiv preprint arXiv:2504.19834*, 2025b.

Xingchao Liu, Chengyue Gong, and Qiang Liu. Flow straight and fast: Learning to generate and transfer data with rectified flow. *ArXiv*, abs/2209.03003, 2022. URL `https://api.semanticscholar.org/CorpusID:252111177`.

Yaofang Liu, Yumeng Ren, Xiaodong Cun, Aitor Artola, Yang Liu, Tieyong Zeng, Raymond H Chan, and Jean-michel Morel. Redefining temporal modeling in video diffusion: The vectorized timestep approach. *arXiv preprint arXiv:2410.03160*, 2024.

Ilya Loshchilov and Frank Hutter. Decoupled weight decay regularization. In *ICLR*, 2019.

Chetwin Low and Weimin Wang. Talkingmachines: Real-time audio-driven facetime-style video via autoregressive diffusion models. *arXiv preprint arXiv:2506.03099*, 2025.

Ben Mildenhall, Pratul P Srinivasan, Rodrigo Ortiz-Cayon, Nima Khademi Kalantari, Ravi Ramamoorthi, Ren Ng, and Abhishek Kar. Local light field fusion: Practical view synthesis with prescriptive sampling guidelines. *ACM Transactions on Graphics (ToG)*, 38(4):1–14, 2019.

Kepan Nan, Rui Xie, Penghao Zhou, Tiehan Fan, Zhenheng Yang, Zhijie Chen, Xiang Li, Jian Yang, and Ying Tai. Openvid-1m: A large-scale high-quality dataset for text-to-video generation. *arXiv preprint arXiv:2407.02371*, 2024.

Shen Nie, Hanzhong Allan Guo, Cheng Lu, Yuhao Zhou, Chenyu Zheng, and Chongxuan Li. The blessing of randomness: Sde beats ode in general diffusion-based image editing. *arXiv preprint arXiv:2311.01410*, 2023.

Muyao Niu, Xiaodong Cun, Xintao Wang, Yong Zhang, Ying Shan, and Yinqiang Zheng. Mofa-video: Controllable image animation via generative motion field adaptions in frozen image-to-video diffusion model. In *ECCV*, 2024.

Xingang Pan, Ayush Tewari, Thomas Leimkühler, Lingjie Liu, Abhimitra Meka, and Christian Theobalt. Drag your gan: Interactive point-based manipulation on the generative image manifold. In *ACM SIGGRAPH 2023 conference proceedings*, pp. 1–11, 2023.

Yatian Pang, Bin Zhu, Bin Lin, Mingzhe Zheng, Francis EH Tay, Ser-Nam Lim, Harry Yang, and Li Yuan. Dreamdance: Animating human images by enriching 3d geometry cues from 2d poses. *arXiv preprint arXiv:2412.00397*, 2024.

Jack Parker-Holder, Philip Ball, Jake Bruce, Vibhavari Dasagi, Kristian Holsheimer, Christos Kaplanis, Alexandre Moufarek, Guy Scully, Jeremy Shar, Jimmy Shi, Stephen Spencer, Jessica Yung, Michael Dennis, Sultan Kenjeyev, Shangbang Long, Vlad Mnih, Harris Chan, Maxime Gazeau, Bonnie Li, Fabio Pardo, Luyu Wang, Lei Zhang, Frederic Besse, Tim Harley, Anna Mitenkova, Jane Wang, Jeff Clune, Demis Hassabis, Raia Hadsell, Adrian Bolton, Satinder Singh, and Tim Rocktäschel. Genie 2: A large-scale foundation world model. 2024. URL https://deepmind.google/discover/blog/genie-2-a-large-scale-foundation-world-model/.

Ziqiao Peng, Wentao Hu, Yue Shi, Xiangyu Zhu, Xiaomei Zhang, Hao Zhao, Jun He, Hongyan Liu, and Zhaoxin Fan. Synctalk: The devil is in the synchronization for talking head synthesis. In *Proceedings of the IEEE/CVF Conference on Computer Vision and Pattern Recognition*, pp. 666–676, 2024.

F. Perazzi, J. Pont-Tuset, B. McWilliams, L. Van Gool, M. Gross, and A. Sorkine-Hornung. A benchmark dataset and evaluation methodology for video object segmentation. In *Computer Vision and Pattern Recognition*, 2016.

Ryan Po, Yotam Nitzan, Richard Zhang, Berlin Chen, Tri Dao, Eli Shechtman, Gordon Wetzstein, and Xun Huang. Long-context state-space video world models. *ICCV*, 2025.

Adam Polyak, Amit Zohar, Andrew Brown, Andros Tjandra, Animesh Sinha, Ann Lee, Apoorv Vyas, Bowen Shi, Chih-Yao Ma, Ching-Yao Chuang, et al. Movie gen: A cast of media foundation models. *arXiv preprint arXiv:2410.13720*, 2024.

Shuhuai Ren, Shuming Ma, Xu Sun, and Furu Wei. Next block prediction: Video generation via semi-auto-regressive modeling. *arXiv preprint arXiv:2502.07737*, 2025.

David Ruhe, Jonathan Heek, Tim Salimans, and Emiel Hoogeboom. Rolling diffusion models. In *ICML*, 2024.

Johannes L Schonberger and Jan-Michael Frahm. Structure-from-motion revisited. In *Proceedings of the IEEE conference on computer vision and pattern recognition*, pp. 4104–4113, 2016.

Jay Shah, Ganesh Bikshandi, Ying Zhang, Vijay Thakkar, Pradeep Ramani, and Tri Dao. Flashattention-3: Fast and accurate attention with asynchrony and low-precision. *Advances in Neural Information Processing Systems*, 37:68658–68685, 2024.

Xiaoyu Shi, Zhaoyang Huang, Fu-Yun Wang, Weikang Bian, Dasong Li, Yi Zhang, Manyuan Zhang, Ka Chun Cheung, Simon See, Hongwei Qin, et al. Motion-i2v: Consistent and controllable image-to-video generation with explicit motion modeling. In *ACM SIGGRAPH 2024 Conference Papers*, pp. 1–11, 2024a.

Yujun Shi, Chuhui Xue, Jun Hao Liew, Jiachun Pan, Hanshu Yan, Wenqing Zhang, Vincent YF Tan, and Song Bai. Dragdiffusion: Harnessing diffusion models for interactive point-based image editing. In *Proceedings of the IEEE/CVF Conference on Computer Vision and Pattern Recognition*, pp. 8839–8849, 2024b.

Joonghyuk Shin, Daehyeon Choi, and Jaesik Park. Instantdrag: Improving interactivity in drag-based image editing. In *SIGGRAPH Asia 2024 Conference Papers*, pp. 1–10, 2024.

Mingzhen Sun, Weining Wang, Gen Li, Jiawei Liu, Jiahui Sun, Wanquan Feng, Shanshan Lao, SiYu Zhou, Qian He, and Jing Liu. Ar-diffusion: Asynchronous video generation with auto-regressive diffusion. In *CVPR*, 2025.

Maham Tanveer, Yang Zhou, Simon Niklaus, Ali Mahdavi Amiri, Hao Zhang, Krishna Kumar Singh, and Nanxuan Zhao. Motionbridge: Dynamic video inbetweening with flexible controls. *arXiv preprint arXiv:2412.13190*, 2024.

Team Wan, Ang Wang, Baole Ai, Bin Wen, Chaojie Mao, Chen-Wei Xie, Di Chen, Feiwu Yu, Haiming Zhao, Jianxiao Yang, Jianyuan Zeng, Jiayu Wang, Jingfeng Zhang, Jingren Zhou, Jinkai Wang, Jixuan Chen, Kai Zhu, Kang Zhao, Keyu Yan, Lianghua Huang, Mengyang Feng, Ningyi Zhang, Pandeng Li, Pingyu Wu, Ruihang Chu, Ruili Feng, Shiwei Zhang, Siyang Sun, Tao Fang, Tianxing Wang, Tianyi Gui, Tingyu Weng, Tong Shen, Wei Lin, Wei Wang, Wei Wang, Wenmeng Zhou, Wente Wang, Wenting Shen, Wenyuan Yu, Xianzhong Shi, Xiaoming Huang, Xin Xu, Yan Kou, Yangyu Lv, Yifei Li, Yijing Liu, Yiming Wang, Yingya Zhang, Yitong Huang, Yong Li, You Wu, Yu Liu, Yulin Pan, Yun Zheng, Yuntao Hong, Yupeng Shi, Yutong Feng, Zeyinzi Jiang, Zhen Han, Zhi-Fan Wu, and Ziyu Liu. Wan: Open and advanced large-scale video generative models. *arXiv preprint arXiv:2503.20314*, 2025.

The FastVideo Team. Github - hao-ai-lab/fastvideo: A unified inference and post-training framework for accelerated video generation. URL `https://github.com/hao-ai-lab/FastVideo`.

Linrui Tian, Qi Wang, Bang Zhang, and Liefeng Bo. Emo: Emote portrait alive generating expressive portrait videos with audio2video diffusion model under weak conditions. In *European Conference on Computer Vision*, pp. 244–260. Springer, 2024.

Yuanpeng Tu, Hao Luo, Xi Chen, Sihui Ji, Xiang Bai, and Hengshuang Zhao. Videoanydoor: High-fidelity video object insertion with precise motion control. In *Proceedings of the Special Interest Group on Computer Graphics and Interactive Techniques Conference Conference Papers*, pp. 1–11, 2025.

Sergey Tulyakov, Ming-Yu Liu, Xiaodong Yang, and Jan Kautz. Mocogan: Decomposing motion and content for video generation. In *CVPR*, 2018.

R Villegas, H Moraldo, S Castro, M Babaeizadeh, H Zhang, J Kunze, PJ Kindermans, MT Saffar, and D Erhan. Phenaki: Variable length video generation from open domain textual descriptions. In *ICLR*, 2023.

Ruben Villegas, Jimei Yang, Seunghoon Hong, Xunyu Lin, and Honglak Lee. Decomposing motion and content for natural video sequence prediction. In *ICLR*, 2017.

Carl Vondrick, Hamed Pirsiavash, and Antonio Torralba. Generating videos with scene dynamics. *NeurIPS*, 2016.

Angtian Wang, Haibin Huang, Jacob Zhiyuan Fang, Yiding Yang, and Chongyang Ma. Ati: Any trajectory instruction for controllable video generation. *arXiv preprint arXiv:2505.22944*, 2025a.

Ruicheng Wang, Sicheng Xu, Yue Dong, Yu Deng, Jianfeng Xiang, Zelong Lv, Guangzhong Sun, Xin Tong, and Jiaolong Yang. Moge-2: Accurate monocular geometry with metric scale and sharp details. *arXiv preprint arXiv:2507.02546*, 2025b.

Wenhao Wang and Yi Yang. Vidprom: A million-scale real prompt-gallery dataset for text-to-video diffusion models. *Advances in Neural Information Processing Systems*, 37:65618–65642, 2024.

Yuqing Wang, Tianwei Xiong, Daquan Zhou, Zhijie Lin, Yang Zhao, Bingyi Kang, Jiashi Feng, and Xihui Liu. Loong: Generating minute-level long videos with autoregressive language models. *arXiv preprint arXiv:2410.02757*, 2024a.

Zhouxia Wang, Ziyang Yuan, Xintao Wang, Yaowei Li, Tianshui Chen, Menghan Xia, Ping Luo, and Ying Shan. Motionctrl: A unified and flexible motion controller for video generation. In *SIGGRAPH*, 2024b.

Dirk Weissenborn, Oscar Täckström, and Jakob Uszkoreit. Scaling autoregressive video models. In *ICLR*, 2020.

Wenming Weng, Ruoyu Feng, Yanhui Wang, Qi Dai, Chunyu Wang, Dacheng Yin, Zhiyuan Zhao, Kai Qiu, Jianmin Bao, Yuhui Yuan, et al. Art-v: Auto-regressive text-to-video generation with diffusion models. In *CVPR*, 2024.

Jianzong Wu, Xiangtai Li, Yanhong Zeng, Jiangning Zhang, Qianyu Zhou, Yining Li, Yunhai Tong, and Kai Chen. Motionbooth: Motion-aware customized text-to-video generation. *Advances in Neural Information Processing Systems*, 37:34322–34348, 2024a.

Rundi Wu, Ruiqi Gao, Ben Poole, Alex Trevithick, Changxi Zheng, Jonathan T Barron, and Aleksander Holynski. Cat4d: Create anything in 4d with multi-view video diffusion models. In *Proceedings of the Computer Vision and Pattern Recognition Conference*, pp. 26057–26068, 2025a.

Tong Wu, Shuai Yang, Ryan Po, Yinghao Xu, Ziwei Liu, Dahua Lin, and Gordon Wetzstein. Video world models with long-term spatial memory. *arXiv preprint arXiv:2506.05284*, 2025b.

Weijia Wu, Zhuang Li, Yuchao Gu, Rui Zhao, Yefei He, David Junhao Zhang, Mike Zheng Shou, Yan Li, Tingting Gao, and Di Zhang. Draganything: Motion control for anything using entity representation. In *European Conference on Computer Vision*, pp. 331–348. Springer, 2024b.

Guangxuan Xiao, Yuandong Tian, Beidi Chen, Song Han, and Mike Lewis. Efficient streaming language models with attention sinks. *arXiv preprint arXiv:2309.17453*, 2023.

Yuxi Xiao, Qianqian Wang, Shangzhan Zhang, Nan Xue, Sida Peng, Yujun Shen, and Xiaowei Zhou. Spatialtracker: Tracking any 2d pixels in 3d space. In *Proceedings of the IEEE/CVF Conference on Computer Vision and Pattern Recognition*, pp. 20406–20417, 2024.

Desai Xie, Zhan Xu, Yicong Hong, Hao Tan, Difan Liu, Feng Liu, Arie Kaufman, and Yang Zhou. Progressive autoregressive video diffusion models. *arXiv preprint arXiv:2410.08151*, 2024.

Jinbo Xing, Hanyuan Liu, Menghan Xia, Yong Zhang, Xintao Wang, Ying Shan, and Tien-Tsin Wong. Tooncrafter: Generative cartoon interpolation. *ACM Transactions on Graphics (TOG)*, 43 (6):1–11, 2024.

Jinbo Xing, Long Mai, Cusuh Ham, Jiahui Huang, Aniruddha Mahapatra, Chi-Wing Fu, Tien-Tsin Wong, and Feng Liu. Motioncanvas: Cinematic shot design with controllable image-to-video generation. In *Proceedings of the Special Interest Group on Computer Graphics and Interactive Techniques Conference Conference Papers*, pp. 1–11, 2025.

Haofei Xu, Songyou Peng, Fangjinhua Wang, Hermann Blum, Daniel Barath, Andreas Geiger, and Marc Pollefeys. Depthsplat: Connecting gaussian splatting and depth. In *Proceedings of the Computer Vision and Pattern Recognition Conference*, pp. 16453–16463, 2025.

Wilson Yan, Yunzhi Zhang, Pieter Abbeel, and Aravind Srinivas. Videogpt: Video generation using vq-vae and transformers. *arXiv preprint arXiv:2104.10157*, 2021.

Yan Team. Yan: Foundational interactive video generation. *arXiv preprint arXiv:2508.08601*, 2025.

Mingyu Yang, Junyou Li, Zhongbin Fang, Sheng Chen, Yangbin Yu, Qiang Fu, Wei Yang, and Deheng Ye. Playable game generation. *arXiv preprint arXiv:2412.00887*, 2024a.

Shiyuan Yang, Liang Hou, Haibin Huang, Chongyang Ma, Pengfei Wan, Di Zhang, Xiaodong Chen, and Jing Liao. Direct-a-video: Customized video generation with user-directed camera movement and object motion. In *ACM SIGGRAPH 2024 Conference Papers*, pp. 1–12, 2024b.

Yuxue Yang, Lue Fan, Zuzeng Lin, Feng Wang, and Zhaoxiang Zhang. Layeranimate: Layer-level control for animation. *arXiv preprint arXiv:2501.08295*, 2025a.

Zhuoyi Yang, Jiayan Teng, Wendi Zheng, Ming Ding, Shiyu Huang, Jiazheng Xu, Yuanming Yang, Wenyi Hong, Xiaohan Zhang, Guanyu Feng, et al. Cogvideox: Text-to-video diffusion models with an expert transformer. In *ICLR*, 2025b.

Tianwei Yin, Michaël Gharbi, Taesung Park, Richard Zhang, Eli Shechtman, Fredo Durand, and Bill Freeman. Improved distribution matching distillation for fast image synthesis. *Advances in neural information processing systems*, 37:47455–47487, 2024a.

Tianwei Yin, Michaël Gharbi, Richard Zhang, Eli Shechtman, Fredo Durand, William T Freeman, and Taesung Park. One-step diffusion with distribution matching distillation. In *Proceedings of the IEEE/CVF conference on computer vision and pattern recognition*, pp. 6613–6623, 2024b.

Tianwei Yin, Qiang Zhang, Richard Zhang, William T Freeman, Fredo Durand, Eli Shechtman, and Xun Huang. From slow bidirectional to fast autoregressive video diffusion models. In *CVPR*, 2025.

Jiwen Yu, Yiran Qin, Xintao Wang, Pengfei Wan, Di Zhang, and Xihui Liu. Gamefactory: Creating new games with generative interactive videos. *arXiv preprint arXiv:2501.08325*, 2025a.

Mark Yu, Wenbo Hu, Jinbo Xing, and Ying Shan. Trajectorycrafter: Redirecting camera trajectory for monocular videos via diffusion models. In *Proceedings of the IEEE/CVF International Conference on Computer Vision (ICCV)*, pp. 100–111, October 2025b.

Wangbo Yu, Jinbo Xing, Li Yuan, Wenbo Hu, Xiaoyu Li, Zhipeng Huang, Xiangjun Gao, Tien-Tsin Wong, Ying Shan, and Yonghong Tian. Viewcrafter: Taming video diffusion models for high-fidelity novel view synthesis. *arXiv preprint arXiv:2409.02048*, 2024.

Lvmin Zhang and Maneesh Agrawala. Packing input frame context in next-frame prediction models for video generation. *arXiv preprint arXiv:2504.12626*, 2025.

Lvmin Zhang, Anyi Rao, and Maneesh Agrawala. Adding conditional control to text-to-image diffusion models. In *Proceedings of the IEEE/CVF international conference on computer vision*, pp. 3836–3847, 2023.

Richard Zhang, Phillip Isola, Alexei A Efros, Eli Shechtman, and Oliver Wang. The unreasonable effectiveness of deep features as a perceptual metric. In *Proceedings of the IEEE conference on computer vision and pattern recognition*, pp. 586–595, 2018.

Tianyuan Zhang, Sai Bi, Yicong Hong, Kai Zhang, Fujun Luan, Songlin Yang, Kalyan Sunkavalli, William T Freeman, and Hao Tan. Test-time training done right. *arXiv preprint arXiv:2505.23884*, 2025a.

Zhenghao Zhang, Junchao Liao, Menghao Li, Zuozhuo Dai, Bingxue Qiu, Siyu Zhu, Long Qin, and Weizhi Wang. Tora: Trajectory-oriented diffusion transformer for video generation. In *CVPR*, 2025b.

Xuanjia Zhao, Jian Guan, Congyi Fan, Dongli Xu, Youtian Lin, Haiwei Pan, and Pengming Feng. Fastdrag: Manipulate anything in one step. *Advances in Neural Information Processing Systems*, 37:74439–74460, 2024.

Guangcong Zheng, Teng Li, Rui Jiang, Yehao Lu, Tao Wu, and Xi Li. Cami2v: Camera-controlled image-to-video diffusion model. *arXiv preprint arXiv:2410.15957*, 2024.

Sixiao Zheng, Zimian Peng, Yanpeng Zhou, Yi Zhu, Hang Xu, Xiangru Huang, and Yanwei Fu. Vidcraft3: Camera, object, and lighting control for image-to-video generation. *arXiv preprint arXiv:2502.07531*, 2025.

Haitao Zhou, Chuang Wang, Rui Nie, Jinlin Liu, Dongdong Yu, Qian Yu, and Changhu Wang. Trackgo: A flexible and efficient method for controllable video generation. In *AAAI*, 2025a.

Jensen Jinghao Zhou, Hang Gao, Vikram Voleti, Aaryaman Vasishta, Chun-Han Yao, Mark Boss, Philip Torr, Christian Rupprecht, and Varun Jampani. Stable virtual camera: Generative view synthesis with diffusion models. *arXiv preprint arXiv:2503.14489*, 2025b.

A TRAINING EFFICIENT TINY VAE

Table A1: **Comparison of Causal VAE Models.** We evaluate reconstruction quality on the Sora demo samples (resized to 81f×832×480) by encoding videos with the Full VAE encoder and decoding with different VAE variants. Our Tiny VAE achieves an order-of-magnitude faster decoding than Full VAEs while outperforming existing community implementations in reconstruction quality.

Model	Decoder Params	Compression Rate	Decoding Time(s) (81×832×480)	PSNR	SSIM	LPIPS
Full VAE (Wan 2.1)	73.3M	8×8×4	1.67	31.43	0.934	0.069
Tiny VAE (Wan 2.1 (Boer Bohan, 2025))	9.84M	8×8×4	0.12	28.85	0.899	0.168
Tiny VAE (Wan 2.1, Ours)	9.84M	8×8×4	0.12	29.27	0.904	0.107
Full VAE (Wan 2.2, 5B)	555M	16×16×4	1.75	31.87	0.938	0.065
Tiny VAE (Wan 2.2, Ours)	56.7M	16×16×4	0.23	28.43	0.883	0.126

As discussed in the main paper, the full CausalVAE becomes a bottleneck in streaming pipelines. Wan 2.1's CausalVAE performs $8\times$ spatial and $4\times$ temporal compression, while Wan 2.2 performs $16\times$ spatial and $4\times$ temporal compression. VAE decoding using the full CausalVAE takes 47% of chunk generation wall time for Wan 2.1 (1.3B), and 35% for Wan 2.2 (5B) in our base setup. Although Wan 2.2 (5B) VAE's higher compression rate enables Wan 2.2 to generate 720P videos in real time, it increases the decoding time and memory footprint.

Inspired by community implementations of Tiny VAE (Boer Bohan, 2025), we train a compact decoder from scratch with larger data, cleaner training pipelines, and better loss designs. While Boer Bohan (2025) trains Tiny VAE by regressing outputs to the original Wan VAE using adversarial loss from a PatchGAN discriminator and reconstruction loss with replay buffer, we extend this design by incorporating LPIPS loss with proper data scaling, and hyperparameter selections. We use a random subset of videos from OpenVid-1M and synthetic Wan videos (total 280K samples), training for 200K steps with a learning rate of 3×10^{-4}, batch size of 16, and AdamW optimizer. We train at a lower resolution of 144×144 and frame length of 21, but the model scales well to larger video dimensions.

As shown in Table A1, Tiny VAE achieves substantially faster decoding with significantly fewer parameters compared to the Full VAE. While Tiny VAEs typically produce slightly lower reconstruction quality than Full VAEs, our implementation substantially outperforms existing community versions. Importantly, when used jointly with our distilled student for latent decoding, we observe minimal quality differences in practice (Table A2), as most quality degradation and drift originate from the diffusion model itself rather than VAE reconstruction. For consistency when evaluating the performance of distilled diffusion model, we use results from Full VAE and report corresponding speed, and adopt Tiny VAE for the streaming demo.

Table A2: **Evaluating Tiny VAE in Streaming Generation Setup.** Using the same distilled student model, we ablate the impact of switching VAE from original Full VAE to Tiny VAE in Sora demo subset. It's important to note that even after changing to Tiny VAE, *our distilled models still outperform all other baselines* and quality differences compared to Full VAEs are marginal while achieving 1.75× and 2.3× higher throughput.

Model	Throughput (FPS)	Latency (s)	PSNR	SSIM	LPIPS
Full VAE (Wan 2.1)	16.7	0.69	16.67	0.531	0.360
Tiny VAE (Wan 2.1, Ours)	29.5	0.39	16.68	0.528	0.365
Full VAE (Wan 2.2, 5B)	10.4	1.14	16.62	0.545	0.343
Tiny VAE (Wan 2.2, Ours)	23.9	0.49	16.62	0.543	0.349

B VBENCH RESULTS AND USER STUDY

We additionally evaluate `MotionStream` using VBench-I2V (Huang et al., 2024) and conduct user studies on 20 samples from the Sora demo subset. In Vbench-I2V, we exclude camera motion

Table A3: **VBench-I2V Results.** We evaluate other baselines using VBench-I2V on Sora subset. While the results primarily depend on the choice of backbone, our models generally achieve high performance across all dimensions.

Method	i2v subject	i2v background	subject consistency	background consistency	motion smoothness	aesthetic quality	imaging quality
Image Conductor (Li et al., 2025e)	0.847	0.868	0.791	0.889	0.906	0.505	0.689
GWTF (Burgert et al., 2025)	0.957	0.974	0.933	0.944	0.981	0.620	0.675
DAS (Gu et al., 2025b)	0.972	0.987	**0.953**	0.958	**0.988**	0.634	0.695
ATI (Wang et al., 2025a)	0.981	0.988	0.948	0.947	0.980	0.629	**0.707**
Ours Teacher (1.3B)	**0.984**	0.988	0.948	0.943	0.987	0.625	0.698
Ours Distilled (1.3B)	0.982	0.987	0.940	0.941	0.985	0.618	0.684
Ours Teacher (5B)	0.983	0.988	0.947	**0.959**	0.982	**0.637**	**0.707**
Ours Distilled (5B)	**0.984**	**0.990**	0.945	**0.959**	0.987	0.630	0.703

and dynamic degree metrics since these dimensions are already constrained by the input trajectory conditions rather than text prompts. VBench results show strong correlation with the underlying backbone model, favoring recent Wan-based architectures. The provision of image and trajectory conditions leads to uniformly high scores across methods, reducing discriminative power between models. Nonetheless, both our teacher and distilled models consistently achieve competitive performance across all evaluated dimensions.

For user study, we collected 2,800 responses evaluating video quality of generated videos using our Wan 2.1 (1.3B) variants. Since accurately assessing track-following capability from thousands of grid point trajectories is challenging for participants, we focused solely on video quality assessment, with results shown in Figure A1. As with VBench, video quality correlates strongly with backbone capacity. Notably, ATI (Wang et al., 2025a), which leverages Wan 2.1 14B (10× larger than our 1.3B model), generally produces more visually favorable videos. However, despite ATI's aesthetic quality, we observe it often lacks precise trajectory adherence. Both our teacher and student models outperform other baselines in quality, with the teacher being slightly preferred over the student.

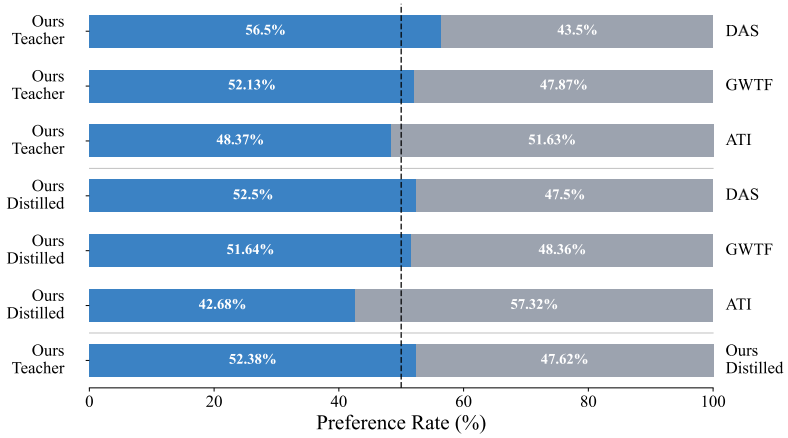
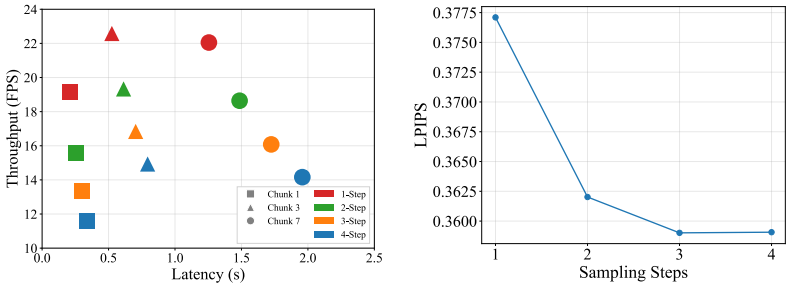


Figure A1: **User Study Results.** We evaluate video quality through pairwise comparisons on 20 Sora samples. In terms of pure video quality, our models outperform all baselines except ATI, which uses a 10× larger backbone (Wan 2.1-14B), producing visually favorable videos.

C Additional Ablation Experiments and Qualitative Results

Impact of Chunk Size and Sampling Steps. In the main paper, we primarily focused on evaluating the efficiency of diverse sparse attention patterns with attention sink size and attention window size. As shown in Table 4 and Figure 6, reducing the chunk size increases the number of autoregressive rollouts required to generate the same length of video while reducing the amount of bidirectional attention, leading to worse performance. Since chunk sizes beyond 3 induce high latency, which makes them less useful for our interactive use case, we report only speed metrics for these configu-



(a) Impact of Chunk Size and Sampling Steps in Throughput and Latency

(b) LPIPS Over Varying Sampling Steps

Figure A2: **Speed and Quality Tradeoffs with Chunk Sizes and Sampling Steps.** We visualize the latency-throughput relationship across varying chunk sizes and sampling steps (left), and image quality (LPIPS) across different sampling steps, using our default setup of `c3s1w1` (right).

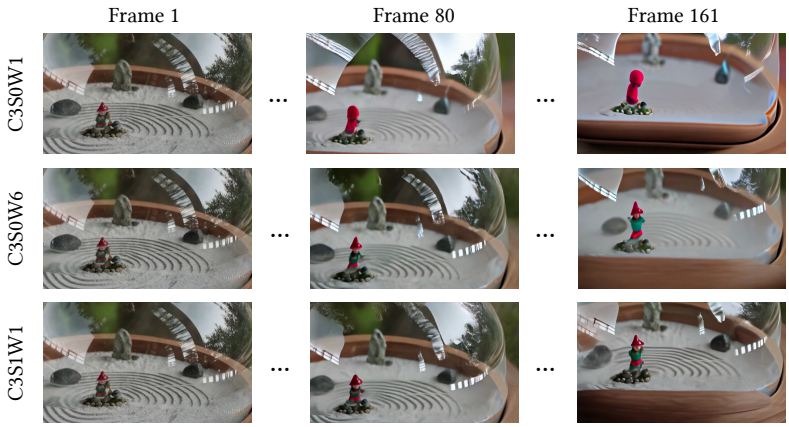


Figure A3: **Long video extrapolation with and without attention sink.** Models without attention sink (top two rows) exhibit cumulative drift over time, while our approach with attention sink (bottom) maintains stable quality throughout extrapolation.

rations. While we did not perform controlled training ablations for larger chunk sizes, we observe similar trends with TalkingMachines (Low & Wang, 2025), where quality generally improves with larger chunks at the cost of latency. Figure A2 (a) visualizes the latency and throughput given different chunk sizes and sampling steps. Note that since all benchmarks are conducted with a sink size and a window size of 1, the model with chunk size 7 has lower FPS than the one with chunk size 3 because its attention sequence length is longer.

The number of sampling steps per chunk also affects this balance. We train our student model for 3-step generation, which we find to be optimal for our motion-controlled setup; increasing beyond 3 steps yields only marginal quality gains, while reducing to 2 steps causes a noticeable drop in quality, as shown in Figure A2 (b). Although trained for 3-step inference, the DMD framework allows for flexible sampling configurations at test time. Based on these findings, we use a chunk size of 3 with 3 sampling steps as our primary configuration to achieve a strong balance between interactivity and high-quality video generation.

Visualization of Attention Sink's Impact on Long Video Extrapolation. We present long video extrapolation results comparing generation with and without attention sinks. As shown in Figure A3, incorporating at least one sink chunk proves crucial for preventing drift during extended generation. Without this, the model exhibits increasing degradation over time, while the attention sink enables stable quality maintenance throughout the video sequence. Please refer to the videos in the supplementary materials for additional results.

Impact of Motion Control on Generative Capability. To assess whether injecting motion control compromises the base model's generative capability, we compare our 1.3B models against the

Table A4: **Impact of Motion Control on Generative Quality.** We evaluate whether injecting motion control degrades the pretrained model's capability by comparing against a larger, dedicated I2V baseline (Wan 2.1 14B I2V). We also report performance when motion conditions are dropped. Results indicate that adding motion conditioning does not significantly degrade the base model's generative quality. While removing motion conditions introduces a slight quality drop as our models were not optimized for this setting, the output still adheres to the given text and image inputs.

Model	i2v subject	i2v bg	subj. consis.	bg consis.	motion smooth.	aesth. qual.	imag. qual.	FVD (↓)
Wan 2.1 I2V (14B)	0.979	0.987	0.947	**0.953**	0.988	0.619	**0.711**	1274.6
Ours Teacher (1.3B) w. Motion	**0.984**	**0.988**	**0.948**	0.943	0.987	**0.625**	0.698	**578.2**
Ours Teacher (1.3B) w/o Motion	0.965	0.976	0.889	0.926	**0.990**	0.613	0.707	1550.4
Ours Student (1.3B) w. Motion	0.982	0.987	0.940	0.941	0.985	0.618	0.684	745.8
Ours Student (1.3B) w/o Motion	0.973	0.982	0.923	0.943	0.986	0.597	0.688	1532.5

larger Wan 2.1 14B I2V baseline, which serves as a high-quality upper bound (as no Wan 1.3B I2V exists) on the Sora dataset. As shown in Table A4, we observe no noticeable degradation; despite the capacity gap and open-source training data, performance remains robust. In fact, a few demo samples demonstrate that motion control enables the model to generate dynamic motions that naive I2V models often struggle to produce due to static bias (Choi et al., 2025). Consequently, FVD scores are lower with motion conditions, as the generated videos better mimic the target distribution through explicit motion constraints.

We also investigate the model's behavior when motion conditions are not provided. Since our models are incentivized to accurately follow motion and are not explicitly trained for an I2V (or "motionless") setup, providing empty motion inputs indeed results in a quality degradation. Nonetheless, while the quality is slightly lower compared to the fully conditioned setting, the model still follows text prompts effectively without severe visual collapse. One interesting observation is that the teacher model without motion conditions rarely produces sudden scene changes, yet results in a lower subject consistency metric. We hypothesize that applying CFG with empty motion conditions leads to unstable outputs where text prompts dominate. We did not observe this behavior with guidance-distilled student models. Please refer to the supplementary videos for detailed results.

Qualitative Comparison. We also provide a qualitative comparison between baselines in Figure A4. Please refer to the supplementary videos for detailed results.

Streaming Demo. We show some examples of our streaming demo in Figure A5. The demo starts by accepting an input image and text prompts, which can help generate effects that are not achievable through mouse drags. Users can then choose the specific spacing/size of the track grids and start controlling objects in a scene, or move the camera. Due to its autoregressive nature, users can pause or resume the streaming generation process. Users can start/end or pause/resume the generation process with `Enter` and `Space` keyboard input, which is especially useful for dynamically adding static grids to specify unmoving regions or multiple moving grids to control different motions during streaming. As a video generative model, our method naturally supports drag-based image editing, generating intermediate transition frames as a bonus, while being faster than most dedicated drag-based image editing methods (Pan et al., 2023; Shi et al., 2024b; Nie et al., 2023; Shin et al., 2024; Zhao et al., 2024). To further support diverse downstream tasks, we will continuously update our front-end UI with additional features.

D Training Details

Data Preprocessing. We train our models on two primary data sources: OpenVid-1M (Nan et al., 2024) and synthetic videos generated by larger Wan text-to-video models. For OpenVid-1M, we filter the dataset to 0.6M videos by requiring a minimum of 81 frames and a 16:9 aspect ratio, sampling at 16 FPS. For synthetic data, we use 70K samples for Wan 2.1 (81 frames, 480P resolution, generated by Wan 2.1 14B using text prompts from VidProm (Wang & Yang, 2024)) and 30K publicly available samples for Wan 2.2 (121 frames, 720P resolution, generated by Wan 2.2 5B from the FastVideo team (The FastVideo Team)).

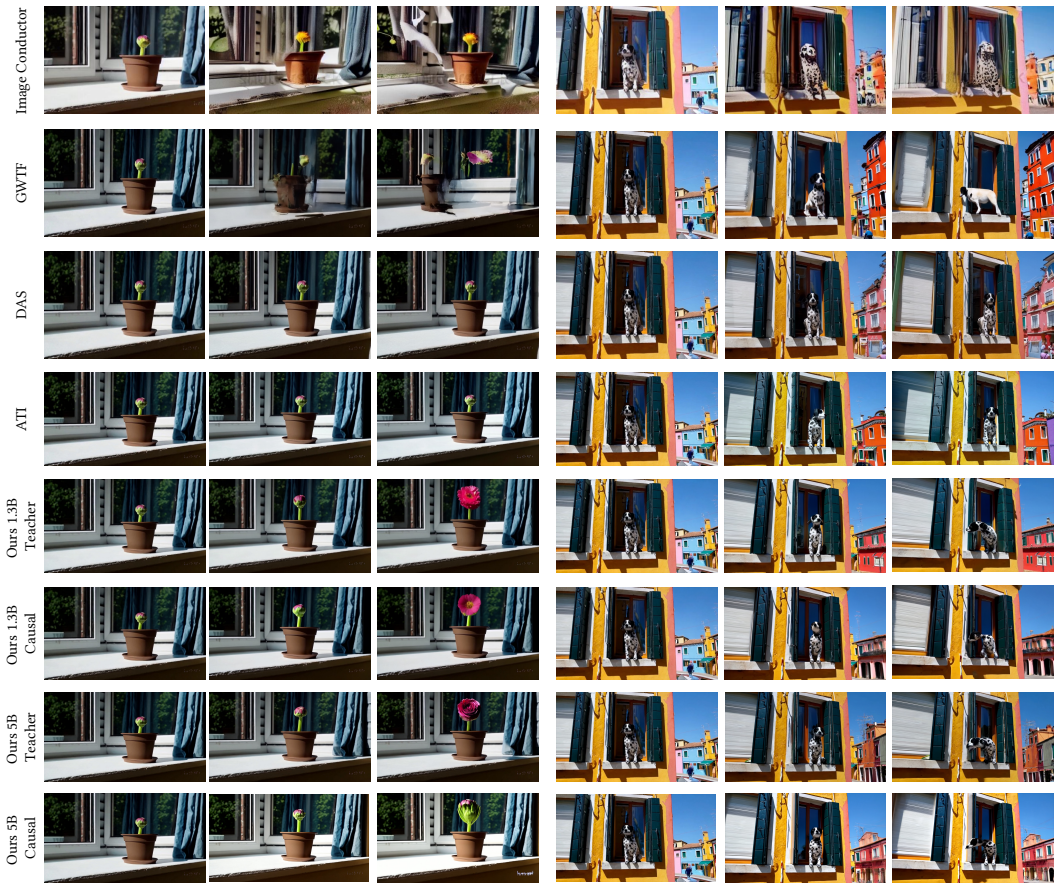


Figure A4: **Qualitative Comparison.** Generated videos from the Sora subset. As seen on the left, our model successfully reconstructs the flower blooming motion, while GWTF captures the motion but suffers quality degradation. ATI produces high-quality videos but with reduced trajectory adherence in motion transfer scenarios.

We extract motion trajectories from all videos using CoTracker3 (Karaev et al., 2024), tracking points on a 50×50 uniform grid. Our training follows a two-stage design: initial training on OpenVid-1M to establish general motion conditioning capability, followed by fine-tuning on cleaner synthetic data to improve trajectory adherence and reduce artifacts from noisy real-world videos. For the distillation phase, we use only synthetic samples since the distillation process converges quickly and requires less data.

For causal adaptation, we generate 4,000 training samples using our joint guidance strategy ($w_t = 3.0, w_m = 1.5$). Notably, Self Forcing-style distillation with DMD objectives does not require complete video sequences during training due to the nature of distribution matching loss design, requiring only the first frame, text prompt, and corresponding motion tracks.

Teacher Model Training. We initialize our teacher models from partial weights of VideoXFun's Wan variants (AIGC-Apps & Alibaba PAI Team, 2024), which extend Wan I2V models with additional control channels. This initialization accelerates convergence compared to training from scratch. Both Wan 2.1 and Wan 2.2 undergo two-stage training: (1) initial training on filtered OpenVid-1M (0.6M videos) for 4.8K steps, followed by (2) fine-tuning on cleaner synthetic data for 800 steps (Wan 2.1) and 400 steps (Wan 2.2), approximately one epoch each. During training, we randomly sample 1,000∼2,500 tracks and assign a sinusoidal positional embedding of $d = 64$ dimensions. Stochastic track masking (described in Sec. 3.1) is applied during the fine-tuning stage. We use batch size 128 with learning rates of 1×10^{-5} and 1×10^{-6} for stages 1 and 2, respectively. The track head remains frozen after initial training as it already operates chunk-wise.

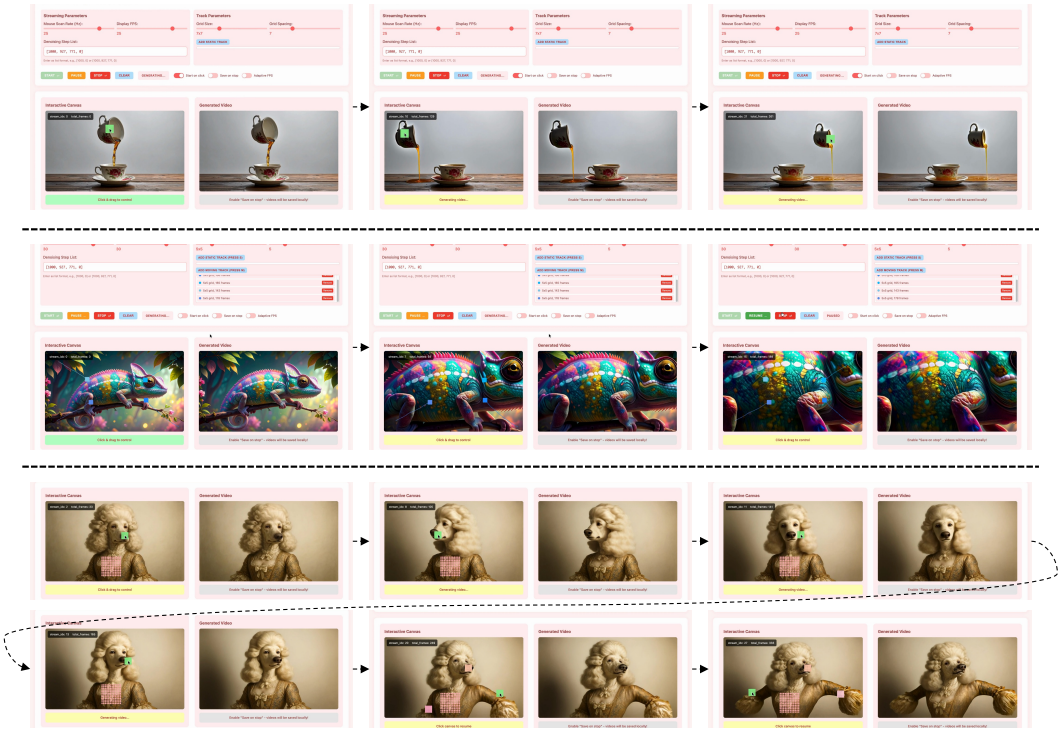


Figure A5: **Streaming Demo.** We show some examples of our streaming demo. Green grids indicate the points that are being dragged (online), red grids indicate a set of points that should remain static, and blue grids indicate user's pre-drawn trajectories for moving multiple points simultaneously (see chameleon example). More examples can be found on our supplementary website.

We train the motion-guided teacher model through rectified flow matching objective, where the forward process linearly interpolates between data z_0 and Gaussian noise $z_1 \sim \mathcal{N}(0, I)$:

$$z_t = (1-t)z_0 + tz_1, \quad t \in [0,1], \tag{A1}$$

with timestep shifting (Team Wan et al., 2025), defined as $t'(k,t) = \frac{kt/1000}{1+(k-1)(t/1000)}$, where $k = 6.0$. The model is trained to predict the expected velocity fields conditioned on noisy latents, denoising time steps, text prompts c_t and motion embedding c_m, with timestep-dependent weighting w_t:

$$\mathcal{L}_{\text{FM}} = \mathbb{E}_{z_0,z_1,t}\left[w_t \left\| v_\theta(z_{t'}, t', c_t, c_m) - (z_1 - z_0)\right\|^2\right]. \tag{A2}$$

Causal Architecture Adaptation. Following CausVid (Yin et al., 2025), we adapt to few-step causal inference through ODE trajectory regression. We generate 4,000 ODE trajectories from the teacher model and train for 2,000 steps. While the transition from bidirectional to causal attention requires significant adaptation, we find variations within causal patterns (e.g., different window sizes) are similar enough to learn jointly with single model. We therefore train with diverse sparse causal attention masks, creating a unified initialization that supports flexible self-rollout configurations. We maintain a batch size of 128 with a learning rate 2×10^{-6}.

Self Forcing-Style Distillation with DMD. Self Forcing distillation converges quickly at around 400 steps with a batch size of 64. We set learning rates to 2×10^{-6} for the generator and 4×10^{-7} for the critic (fake score function), with a 1:5 update ratio and gradient truncation as described in Sec. 3.2.

We employ AdamW optimizer (Kingma & Ba, 2015; Loshchilov & Hutter, 2019) with mixed precision (bfloat16) and PyTorch's FSDP. Exponential moving average (EMA) is applied during teacher training and DMD distillation. Wan 2.1 variants train at 832×480 resolution while Wan 2.2 trains at 1280×704. With 32 A100 GPUs, training the Wan 2.1 teacher model takes roughly 3 days with

causal adaptation and distillation completing in 20 hours, while Wan 2.2 requires slightly longer training times.

E Evaluation Protocols

Since different methods employ various backbone models with different spatial and temporal resolutions, we optimize the evaluation setup for each method by matching their primary spatial/temporal dimensions. For DAVIS evaluation, when the number of frames exceeds a model's default temporal length, we retain the first and last frames while uniformly subsampling intermediate frames, then compare against correspondingly subsampled ground truth frames.

All Sora demo videos were limited to 81 frames at 16 FPS for standard experiments, except for the extrapolation experiments in Table 4 and Figure 6, which use up to 241 frames (average 194 frames, approximately 15 seconds). Similar subsampling was applied for models with shorter temporal contexts (16 frames for AnimateDiff, 49 for CogVideoX).

We report the best scores for each method using its optimal configuration. For Image Conductor, we tested with 1, 10, 100, 1000, 2500 tracks and report results from 100 tracks, which performed best. Go-With-The-Flow requires dense optical flow as input, so we provide flow estimated by RAFT following their reference implementation. Diffusion-As-Shader uses 3D tracks as input, for which we provide tracks from SpatialTracker (Xiao et al., 2024) on a 70×70 grid (their default setting). ATI was tested with 40, 2500 tracks, and we report results from 40 tracks (their default), which performed better. Our models consistently use 2D trajectories from 50×50 initial grid points tracked by CoTracker3.

After generation, all results are resized to 832×480 resolution to ensure a consistent scale for metrics, particularly EPE which calculates L2 distance between track coordinates. All latency and throughput are measured using a single H100 GPU in bfloat16 precision with Flash Attention 3 (Shah et al., 2024).

For the camera control benchmark on the LLFF dataset, we derive 50×50 grid tracks using the method described in Sec. 4.2. To minimize unintended object motion and focus the evaluation purely on camera movement, we use the prompt template: "static scene, only camera motion, no object is moving, {`scene_name`}", where {`scene_name`} is replaced with the specific LLFF scene name.

F Limitation and Future Work

While MotionStream achieves real-time motion control for long-range video generation, we identify several limitations. First, the fixed attention sink mechanism, while ensuring stable long-term generation, constrains the model's ability to handle scenarios with complete scene changes. Our approach maintains strong anchoring to the initial chunk, which works well for most motion-controlled generation scenarios where cameras and objects move within consistent environments. However, when presented with trajectories from game engines or other sources where environments change continuously, the model exhibits a tendency to preserve the initial scene rather than adapting to new contexts. This limitation is also inherent to current 2D tracking systems, which cannot meaningfully track and encode complete scene transitions. Future work could explore dynamic attention sinking strategies that adaptively refresh anchor frames for world modeling applications.

Second, we observe artifacts when motion trajectories are extremely rapid or physically implausible, manifesting as temporal inconsistencies or distortions in object appearance. One good approach for future work would be exploring effective track augmentation strategies during training to better simulate imperfect user inputs and scaling to larger backbone models, which generally exhibit more robust visual quality.

Lastly, our pipeline sometimes struggles to preserve source details when scenes, text prompts, or intended motions are highly complex. This primarily stems from backbone capacity limitations. While motion conditioning with text prompts can enforce movements beyond what the base model generates from text alone, quality may be unsatisfactory in such cases. We also note that different image conditioning mechanisms across different backbones can affect the robustness of the model in handling imperfect motion cues. Interestingly, we empirically observed that the smaller Wan 2.1 (1.3B)

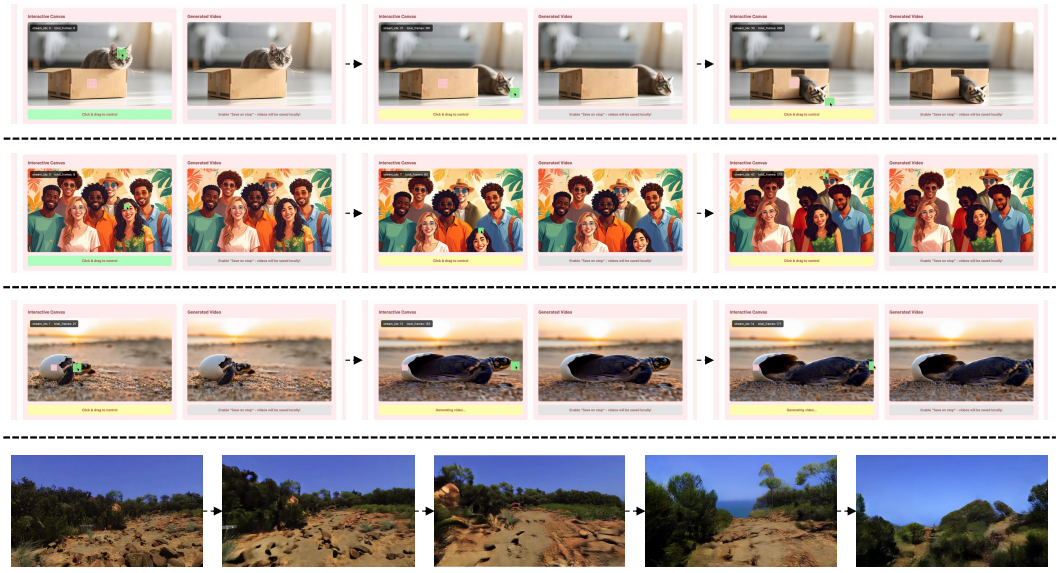


Figure A6: **Failure Cases.** In the cat and turtle examples, the intention was to bring the cat out of the box and make the turtle hatch from the egg. However, due to limitations in hand-drawn trajectories for expressing complex motions and the backbone model's generalization capacity, the outputs are not physically plausible, and objects are either deformed or simply translated along the tracks. In complex scenes with multiple human identities (second example), the model often loses identity information and produces artifacts. The last row shows our model's output on the world exploration task. Since track representation struggles to capture complete scene transitions and the attention sink prioritizes preserving source features, our pipeline faces difficulty in scenarios where new objects appear or scenes continuously change. More videos can be found on our supplementary website.

usually outperforms Wan 2.2 (5B) in preserving source structures, particularly with user-drawn flat-grid imperfect point trajectories. We attribute this to Wan 2.1's input image cross-attention design which helps maintain the original structure throughout, while Wan 2.2's TI2V structure is slightly more experimental. As our models are relatively modest in scale, we expect larger base models to provide improved performance and stability under challenging scenarios. Some of our failure cases can be found in Figure A6.

G Ethics Statement

As video generative models become increasingly capable of producing realistic content that mimics world dynamics, we recognize the potential for misuse. While `MotionStream` advances interactive content creation with intuitive controls, our approach naturally inherits potential risks from the underlying generative technology, including the creation of deceptive media. We emphasize the critical need for parallel development of safeguarding techniques such as watermarking, content authentication, and controlled access mechanisms. We encourage prioritizing responsible deployment strategies alongside capability improvements to ensure these tools benefit society while minimizing harms.

Reproducibility. Our models are built upon publicly available Wan model variants and datasets (OpenVid-1M and synthetic Wan videos). Training was conducted in a well-controlled environment, with all training details, hyperparameters, and implementation specifics provided in Sec. D and the supplementary to ensure reproducibility.

LLM Usage. We used LLMs to help polish the writing and presentation of this manuscript. LLMs were not used for research ideation, experimental design, or scientific discovery in this work.